

Accounting for Skill in Nonlinear Trend, Variability, and Autocorrelation Facilitates Better Multi-Model Projections

Roman Olson^{a,b,c}, Soon-Il An^a, Yanan Fan^d and Jason P. Evans^e

^aDepartment of Atmospheric Sciences, Yonsei University, Seoul, South Korea, 03722

^bCenter for Climate Physics, Institute for Basic Science, Busan, South Korea, 46241

^cPusan National University, Busan, South Korea, 46241

^dSchool of Mathematics and Statistics, UNSW, Sydney, NSW, 2052, Australia

^eClimate Change Research Centre and ARC Centre for Excellence in Climate Extremes, UNSW Australia, Sydney, NSW, Australia

Abstract

We present a novel quasi-Bayesian method to weight multiple dynamical models by their skill at capturing both non-linear trend and first-order autocorrelated variability, and to make weighted probabilistic projections. In validation experiments the method tends to exhibit superior skill over a trend-only weighting method in terms of weight assignment and probabilistic forecasts. Specifically, mean credible interval width, and mean absolute error of the projections tend to improve. We apply the method to a problem of projecting summer mean temperature change over Korea by the end of the 21st century using a multi-model ensemble. Compared to the trend-only method, the new method appreciably sharpens the probability distribution function (pdf) and increases future most likely, median, and mean warming in Korea. The method is flexible, with a potential to improve forecasts in geosciences and other fields.

1 Introduction

A common forecasting problem is one of probabilistic multi-model forecasts of a stochastic dynamical system (Bhat et al., 2011; Buser et al., 2009; Christoph M. Buser et al., 2010; Chandler, 2013; Duan et al., 2007; Huttunen et al., 2017; Knutti, 2008; Olson et al., 2016, 2017; Raftery et al., 2005; Rougier et al., 2013; Steinschneider et al., 2015; Tebaldi et al., 2011; Tebaldi & Sansó, 2009; Terando et al., 2012; Wallach et al., 2016; Xu et al., 2010). A forecaster has a collection of complex dynamical models at hand, which are weighted according to their performance compared to observations, and the weights are then used to provide weighted multi-model forecasts (Acharya et al., 2014; Bhat et al., 2011; Duan et al., 2007; Hoeting et al., 1999; Montgomery & Nyhan, 2010; Raftery et al., 2005; Yun et al., 2003, 2005). The Bayesian approach to this problem assumes that associated with k dynamical models are k competing statistical models M_i for vector of observations \mathbf{y} . These statistical models result in a conditional probability density function (pdf) for \mathbf{y} given that M_i is reasonable $p(\mathbf{y}|M_i)$. Typically, in multi-model evaluation context, the pdf $p(\mathbf{y}|M_i)$ is a multivariate statistical distribution centered on i th dynamical model trend \mathbf{x}_i . The researcher has a prior belief in each model (“prior”) $p(M_i)$, which can be derived from previous work, or be more subjective. The posterior probability, or weight, for each model i given the observations is then found using Bayes theorem (Bayes & Price, 1763):

$$p(M_i|\mathbf{y}) \propto p(\mathbf{y}|M_i)p(M_i) \quad (1)$$

Specifically, the posterior probability of each statistical (and corresponding dynamical) model is the likelihood of observations \mathbf{y} coming from the model [given by the pdf $p(\mathbf{y}|M_i)$], multiplied by the model prior.

In ensemble modelling, models are usually judged on how well they represent the mean state of the system, its trend, or spatio-temporal fields (Bhat et al., 2011; Buser et al., 2010; Huttunen et al., 2017; Tebaldi & Sansó, 2009; Yun et al., 2003, 2005). However, it is increasingly being recognized that variability is of utmost importance for future prediction. Specifically, for some systems (stochastic dynamical systems) the stationary pdf of the equilibrium solution is directly affected by system dynamics (i.e., the nonlinear operator in the ordinary differential equations) through the so-called Fokker-Planck equations. Recent climate science work identifies variability as a key factor impacting climate projections (Fischer et al., 2012; Huttunen et al., 2017). Cox (2018) has used variability as a novel and effective constraint for climate sensitivity.

Variability also has major relevance for forewarning of critical thresholds (i.e., a forcing value above which the underlying system shifts to a new equilibrium; Kopp et al., 2016). Specifically, an increase in variance or lag-1 autocorrelation with time, as well as skewness and kurtosis, have been used as such early warning indicators (Feng et al., 2014; Kleinen et al., 2003; Lenton, 2012; Thomas 2016). This motivates using variability properties of the system as a novel metric to assess multiple dynamical system models.

Thus, several new studies start to incorporate variability into the weighting (e.g., Braverman et al., 2011; Kwasniok, 2013; Peavoy & Franzke, 2016; Xu et al., 2010). These approaches break important new ground. However, they typically assume stationarity of the pdf of the system (Braverman et al., 2011; Kwasniok, 2013; Xu et al., 2010), or cannot work with complex dynamical models (Peavoy & Franzke, 2010). Fan et al. (2017) do explicitly weight dynamical models by performance in variability and trends in a statistically-sound way. However, the method in its current form works only for linear trends and does not account for autocorrelation in the variability.

Here we propose a novel method to weight models of complex dynamical systems by their performance in autocorrelation, variability, and nonlinear trend compared to observations, and to make probabilistic forecasts. The method is based on Bayesian Model Averaging (BMA) (Hoeting et al., 1999; Montgomery and Nyhan, 2010). While the framework is Bayesian, it deviates from traditional Bayesian theory in some steps of the estimation process. We highlight these deviations where they arise in more detail in further sections. Consequently, we call our approach “quasi-Bayesian”. Using several simulated and observed datasets we show that the new method results in better weighting and tends to improve forecasts of system mean change under new conditions compared to when trend-only weighting is used. Thus, this work has implications for improving projections of many environmental systems. The approach is not restricted to linear trends, making it relatively easy to apply to new datasets.

2 Materials and Methods

2.1 Decomposition of Model Output

We postulate that each dynamical model is associated with a statistical model M_i for the observations. M_i can be thought of as a statistical event, which when true indicates that i th dynamical model is a reasonable representation of real system. M_i consists of two submodels: a trend submodel $M_{T,i}$ (related to the trend in the system), and a variability submodel $M_{V,i}$ (modelling internal fluctuations in the system). When $M_{T,i}$ is true, the i th dynamical model correctly captures the trend of the system. Likewise, $M_{V,i}$ when true means that i th dynamical model correctly captures the variability of the system. Alternatively, we can consider the model for fluctuations scaled by the mean ($M_{V0,i}$). The weights (or probabilities) for the two submodels are calculated separately, using the Bayesian statistical paradigm, and then combined. The combined weights can then be used to make predictions (Figure 1).

Consider that k models are available. Each model produces time series output of a physical quantity during the period when observations are available (“calibration period”), as well as under new forcing conditions, usually associated with future system projections (“projection period”). We are interested to find the probability distribution of a change of the system mean Δ between a “projection reference period” (typically the same as the calibration period) and the projection period. We denote the raw calibration period model output from the i th dynamical model by vector

$\mathbf{x}'_i = (x'_{i,1}, \dots, x'_{i,n})$ where superscript “ $'$ ” indicates that the output is raw (un-smoothed), and n is the length of the record. The model output is a regularly spaced time series. We consider decomposition of the form:

$$\mathbf{x}'_i = \underbrace{\mathbf{x}_i}_{\text{trend}} + \underbrace{\Delta \mathbf{x}_i}_{\text{fluctuations}} \quad (2)$$

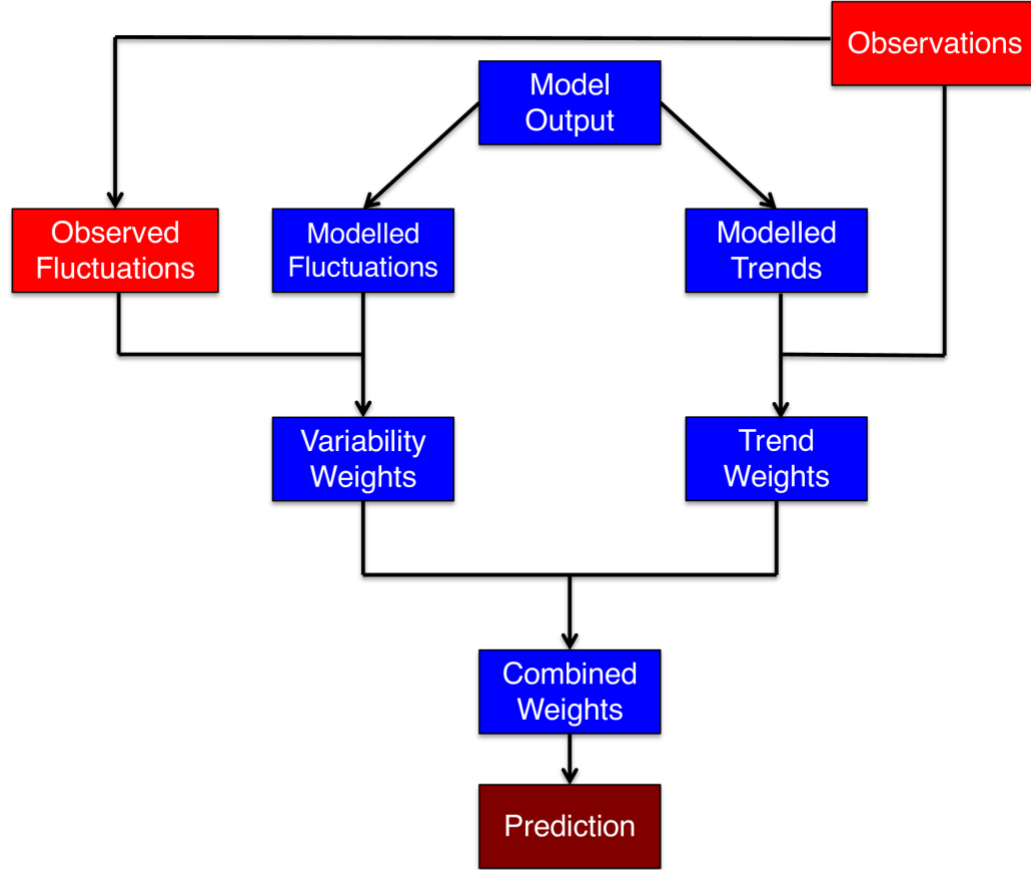


Figure 1. Schematic illustrating the proposed “trend+var” method.

We will use the term “fluctuations” to refer to the variability component of the time series. The trend \mathbf{x}_i can be either a linear trend, or a more flexible nonlinear trend obtained, for example, from robust locally weighted regression (Cleveland, 1979). We assume that this decomposition is deterministic, unique, and is performed before the start of the main analysis. We also assume that the estimate of the trend is a reasonable proxy for the true unknown trend. While it may be possible to also incorporate the uncertainty in this decomposition, we leave it to future work. The focus here is not on how to properly decompose a time series into a long-term trend and variability, but on the weighting by performance in both. We describe the decomposition method we use for each dataset in Section 3. The same decomposition is also applied to the observed time series \mathbf{y}' :

$$\mathbf{y}' = \mathbf{y} + \Delta \mathbf{y}. \quad (3)$$

Another option is relative decomposition. It takes the following form:

$$\mathbf{x}'_i = \underbrace{\mathbf{x}_i}_{\text{trend}} + \underbrace{\bar{\mathbf{x}}_i \Delta \mathbf{x}_i^0}_{\text{fluctuations}}, \quad (4)$$

where $\bar{\mathbf{x}}_i$ is the deterministic sample mean of the i th dynamical model output, and $\Delta \mathbf{x}_i^0$ are normalized fluctuations; and similarly for the observations:

$$\mathbf{y}' = \mathbf{y} + \bar{\mathbf{y}} \Delta \mathbf{y}_i^0, \quad (5)$$

where $\bar{\mathbf{y}}$ is the observed mean.

2.2 Weighting the Trend Submodels

Here, we consider k competing statistical models $M_{T,i}$ for raw observations \mathbf{y}' . We stress that statistical and dynamical models are conceptually related: i.e., if the statistical model $M_{T,i}$ is true, it implies that the associated i th dynamical model correctly represents the trend in the system. The trend submodel weighting is implemented following Olson et al. (2017), and full details are provided there. Each $M_{T,i}$ is a hierarchical statistical model that connects modelled deterministic trend from the i th model during the calibration period \mathbf{x}_i to real system trend \mathbf{y} (Eq. (6a)), and then the system trend to actual observations \mathbf{y}' (Eq. (6b)):

$$\begin{cases} \mathbf{y} = \mathbf{x}_i + f \boldsymbol{\varepsilon}_D \end{cases} \quad (6a)$$

$$\begin{cases} \mathbf{y}' = \mathbf{y} + \boldsymbol{\varepsilon}_{NV}, \end{cases} \quad (6b)$$

where $f \boldsymbol{\varepsilon}_D$ is random discrepancy (long-term model error), and $\boldsymbol{\varepsilon}_{NV}$ is random internal variability (as well as short-term observational error).

Here we deviate somewhat from orthodox Bayesian practice. A typical Bayesian approach would assume a distributional form for the discrepancy vector $f \boldsymbol{\varepsilon}_D$. However, because this error is likely long-term dependent, and the probability distributions for its components are not necessarily normal, finding and justifying a proper parametric model for it is non-trivial. To deal with this conundrum, we adopt an approach inspired by Sexton et al. (2012). We postulate that model error is related to inter-model trend differences (e.g., model error is smaller for years when models predict similar output, and larger for years when model trends considerably diverge). Thus, we obtain samples for unscaled discrepancy $\boldsymbol{\varepsilon}_D$ directly from the differences between each model's trend and the next-closest model trend. The reasoning for this implementation is as follows. Imagine a particular trend submodel $M_{T,i}$ represents the “true” system. Associated with this system is trend \mathbf{x}_i . If only the rest of the models are available to the researcher, then the best-fit model j to these pseudo-observations is associated with trend \mathbf{x}_j . The difference between the two trends is then the unscaled error of the j th model.

The second non-orthodox idea, is related to the deterministic f factor (“error expansion factor”), introduced here, which is a deterministic parameter that scales $\boldsymbol{\varepsilon}_D$ to account for potential overconfidence. We believe that no matter whether long-term error is parameterized in terms of some parameters which are estimated directly using observations (a more Bayesian approach), or whether it is derived from inter-model differences, the estimation may be biased. In the former case, because of potential overfitting, the model-observational distance may be an underestimate of the actual model error. In the latter case, as all models may share common errors, the inter-model differences may also underestimate model error. In any case, too optimistic error estimates are expected to result in large weights for only one or few models, and in overconfident multi-

model projections. At the same time, too broad estimates are expected to produce similar weights for all models. It is impossible to correctly gauge the magnitude of model error by looking at present-day observations alone; we need some other information. Thus, the magnitude of ϵ_D needs to be scaled to correct for potential overconfidence. As will be described in more detail in forthcoming sections, here we use one-at-a-time cross-validation framework, and compare projection period model output for each model to multi-model projections from the remaining models. We calibrate f to provide reasonable empirical coverage during the cross-validation.

The internal variability ϵ_{NV} is modelled as an AR(1) process with random parameters $\theta = (\sigma, \rho)$, where σ is innovation standard deviation and ρ is autocorrelation. Following Bayes theorem, and marginalization theorem, the trend model weights are then calculated as:

$$p(M_{T,i}|\mathbf{y}') \propto p(M_{T,i}) \iint p(\mathbf{y}'|\mathbf{y}, \theta, M_{T,i}) p(\theta) p(\mathbf{y}|M_{T,i}) d\mathbf{y} d\theta. \quad (7)$$

Here, $p(M_{T,i})$ denotes the prior for the i th trend model, $p(\mathbf{y}'|\mathbf{y}, \theta, M_{T,i})$ is the AR1 likelihood resulting from Eq. (6b), $p(\theta)$ denotes the prior for the AR1 parameters, and $p(\mathbf{y}|M_{T,i})$ is obtained according to Eq. (6a) using samples from $f\epsilon_D$ as discussed above. Unlike in Olson et al. (2017), here we assume uniform prior probabilities for trend models $p(M_{T,i})$. The integral is evaluated using Monte Carlo integration, which is simpler to implement than Markov chain Monte Carlo methods used in some studies (Buser et al., 2009). For the relative low dimension parameter space that we deal with here, simple Monte Carlo is adequate. Additional experiments suggest the sample size we use for the Monte Carlo integration is reasonable to minimize Monte Carlo error (Supporting Text S1). Once calculated, the weights are normalized to sum to 1 to facilitate interpretation as probabilities. We provide technical details in Supporting Text S1.

2.3 Weighting the Variability Submodels

Variability model is weighted using similar ideas to the ones used in trend weight estimation. We consider k competing statistical models for calibration period fluctuations observations $\Delta\mathbf{y} = (\Delta y_1, \Delta y_2, \dots, \Delta y_n)$ (see Eq. (3)). Each i th variability model $M_{V,i}$ models the fluctuations hierarchically in the following form:

$$\begin{cases} \theta_y^V = \check{\theta}_{M,i}^V + f\epsilon^V \end{cases} \quad (8a)$$

$$\Delta y_t = \rho_y \Delta y_{t-1} + w_t, \quad (8b)$$

where $w_t \sim N(0, \sigma_y^2)$. First, in Eq (8a) instead of performing full posterior sampling to obtain samples for real system autocorrelation and innovation standard deviation parameters $\theta_y^V = (\sigma_y, \rho_y)$, we assume they are centered around summary statistics $\check{\theta}_{M,i}^V = (\check{\sigma}_{M,i}, \check{\rho}_{M,i})$ of i th physical model fluctuations with an additive error $f\epsilon^V$. Again, we refrain from assuming any parametric form for this distribution. Each model's summary statistics are taken as the corresponding MLE estimates. Furthermore, $\epsilon^V = (\epsilon_\sigma, \epsilon_\rho)$ is the random unscaled discrepancy term and f is a deterministic scaling factor to widen the distribution to correct for potential overconfidence. This is the same parameter that is used to scale trend model discrepancy (Section 2.2). Loosely following Olson et al (2017) we assume samples for ϵ^V are obtained from differences between each model summary statistics and the next-closest model summary statistics. The next-closest model is found as follows: for each model i we compare $p(\Delta\mathbf{x}_i|\check{\theta}_{M,j}^V)$, $j \neq i$ under the AR(1) statistical model, and find j that maximizes this likelihood. We also add a sample of zero

vector (0,0) to $\boldsymbol{\varepsilon}^V$ for computational stability. This approach gives us only $k+1$ samples from $f\boldsymbol{\varepsilon}^V$. To obtain a larger number of samples which are well-dispersed, we add to $f\boldsymbol{\varepsilon}^V$ realizations from an independent bivariate normal distribution with standard deviations set to 1/5 of the initial sample ranges. We use the value of 1/5 because it results in samples with a reasonably smooth density that preserves large scale cross-correlation structure between the original non-nudged samples of ε_σ and ε_ρ , and provides a decent approximation in our view to the underlying pdf for $f\boldsymbol{\varepsilon}^V$ (Figure S1). Sensitivity tests indicate that using lower standard deviations can degrade the smoothness of the pdf (not shown).

In the second step (Eq. 8(b)) we assume the fluctuations observations during the calibration period are modelled by an AR1 process with autocorrelation ρ_y and innovation standard deviation σ_y .

Then, the posterior probability of the variability model i is, using Bayes rule (Bayes & Price, 1763) and probability rules:

$$p(M_{V,i}|\Delta\mathbf{y}) = \int p(M_{V,i}, \boldsymbol{\theta}_y^V|\Delta\mathbf{y}) d\boldsymbol{\theta}_y^V \propto p(M_{V,i}) \int p(\Delta\mathbf{y}|M_{V,i}, \boldsymbol{\theta}_y^V) p(\boldsymbol{\theta}_y^V|M_{V,i}) d\boldsymbol{\theta}_y^V, \quad (9)$$

where $p(\Delta\mathbf{y}|M_{V,i}, \boldsymbol{\theta}_y^V)$ is an AR1 likelihood function, $p(\boldsymbol{\theta}_y^V|M_{V,i})$ is sampled using Eq. 8(a) using bootstrapping from $f\boldsymbol{\varepsilon}^V$ as described above, and $p(M_{V,i})$ is the prior probability (“prior”) for the i th variability submodel. We assume equal priors for all submodels. This integral is also evaluated using Monte Carlo integration. Specifically, we sample from conditional pdf of real system summary statistics given each variability model $p(\boldsymbol{\theta}_y^V|M_{V,i})$ as described above, and for each sample we calculate the conditional likelihood for the fluctuations observations $p(\Delta\mathbf{y}|M_{V,i}, \boldsymbol{\theta}_y^V)$. The integral is approximated as a simple mean of the conditional likelihoods across the samples. Probabilities are calculated for each submodel and are normalized to sum up to 1. The implementation using relative variability M_{V0} is identical except the residuals $\Delta\mathbf{x}_i$ and $\Delta\mathbf{y}$ are normalized by the respective model and observational means prior to the analysis. We provide technical details on the implementation in Supporting Text S2.

2.4 Combined Weights and Bayesian Model Averaging

In the next step, the weights for the two submodels are combined. Using probability laws:

$$p(M_i|\mathbf{y}, \Delta\mathbf{y}) = p(M_{T,i}, M_{V,i}|\mathbf{y}, \Delta\mathbf{y}) = p(M_{T,i}|M_{V,i}, \mathbf{y}, \Delta\mathbf{y}) \times p(M_{V,i}|\mathbf{y}, \Delta\mathbf{y}). \quad (10)$$

We make two simplifying assumptions. First, we observe that in the datasets described in Section 3 typically the relationships between the variability summary statistics $\check{\sigma}_{M,i}$ and $\check{\rho}_{M,i}$ on one hand, and trend model probability on the other hand, appear to be weak (Figures S2-S11). In addition, the corresponding linear coefficients are almost always weak (weak is defined as the absolute values less than 0.5). Assuming that the relationships based on the sample summary statistics are a good proxy for those based on the population properties, we make an assumption that the probability of the trend model is independent of the variability model:

$$p(M_{T,i}|M_{V,i}, \mathbf{y}, \Delta\mathbf{y}) \approx p(M_{T,i}|\mathbf{y}, \Delta\mathbf{y}) = p(M_{T,i}|\mathbf{y}'), \quad (11)$$

which allows us to directly plug in trend model weights obtained using the method in Section 2.2. Second, since only fluctuations are used to weight the variability model:

$$p(M_{V,i}|\mathbf{y}, \Delta\mathbf{y}) = p(M_{V,i}|\Delta\mathbf{y}). \quad (12)$$

This quantity is obtained following Section 2.3. As a result, the combined weights can be expressed as a product of the trend and variability submodel weights:

$$p(M_i|\mathbf{y}, \Delta\mathbf{y}) = p(M_{T,i}|\mathbf{y}, \Delta\mathbf{y}) \times p(M_{V,i}|\Delta\mathbf{y}). \quad (13)$$

We stress that even though the independence assumption generally appears reasonable here, it may not always apply. Hence, it is recommended to check it when applying the methodology to new datasets. Incorporating the potential dependence between the trend and variability submodels into our framework is the subject of future research. Once calculated, the probabilities are normalized to sum up to 1, meaning that we restrict our probability space to the union of available models M_i .

2.5 Future Projections

Once the weights are obtained, the statistical model for system change between projection reference and projection periods Δ follows the BMA formula (Hoeting et al., 1999; Montgomery & Nyhan, 2010):

$$p(\Delta|D) = \sum_{i=1}^k p(\Delta|M_i, D)p(M_i|D) = \sum_{i=1}^k w_i p(\Delta|M_i, D), \quad (14)$$

where $D = (\mathbf{y}, \Delta\mathbf{y})$ is collection of all available observations, $p(\Delta|M_i, D)$ is conditional probability for the change given than i th dynamical model is correct, and $w_i = p(M_i|D)$ is the probability for the i th model (i.e., model weight) found earlier (Eq. (13)) as the product of the trend and variability model probabilities. This represents a skill-weighted mixture of pdfs from individual models. Here we consider Δ to be a simple difference between projection period mean and forecast reference period mean. Future predictions are largely modelled following prior work (Olson et al., 2017). Just as for the calibration period, we assume a deterministic decomposition of projection period output into trend and fluctuations:

$$\mathbf{x}_i'^{(f)} = \underbrace{\mathbf{x}_i^{(f)}}_{\text{trend}} + \underbrace{\Delta\mathbf{x}_i^{(f)}}_{\text{fluctuations}} \quad (15)$$

The exact decomposition method for each dataset is listed in Section 3. Next, we consider the following statistical model for dynamical system time-series projections (all quantities are vectors):

$$\mathbf{y}'^{(f)} = \mathbf{x}_i^{(f)} + \mathbf{b}^{(f)} + \boldsymbol{\varepsilon}_{S,i}^{(f)}, \quad (16)$$

where $\mathbf{y}'^{(f)}$ is the projection time series, $\mathbf{x}_i^{(f)}$ is i th model trend output from Eq. (15), $\mathbf{b}^{(f)} = b^{(f)}\mathbf{1}$ is random time-constant bias, and $\boldsymbol{\varepsilon}_{S,i}^{(f)}$ is random short-term internal variability in each model. Thus, we assume that if i th model is correct, the vector projection is the sum of i th model trend, a time constant bias, and internal variability. Here we again deviate somewhat from the traditional Bayesian theory in that the components of this model are partially informed by inter-model differences, and by model output during cross-validation experiments. Such steps are necessitated by the absence of actual system observations over the projection period to inform us about these components. We model the bias parameter as $b^{(f)} \sim N(0, f\tilde{\sigma}_b^{(f)})$ where $\tilde{\sigma}_b^{(f)}$ is sample standard deviation of future period-mean next-best model differences (where next-best is used in the l_1 distance sense), and f is the deterministic model error expansion factor (the same factor that is used for model weighting). Two different formulations are implemented for internal variability. In the

first formulation (“boot”) (Olson et al., 2017) we use simple bootstrapping from $\Delta \mathbf{x}_i^{(f)}$ to generate internal variability samples. In the alternative formulation (“ar1”) we sample $\boldsymbol{\varepsilon}_{S,i}^{(f)}$ as a red noise process with parameters $\boldsymbol{\theta}_i^{(f)} = (\check{\sigma}_i^{(f)}, \check{\rho}_i^{(f)})$, the sample innovation standard deviation and autocorrelation of future fluctuations. An improvement would be to consider the uncertainty in the AR1 parameter; we do not do this here to simplify the method. To obtain projection period mean changes from the reference period, we take weighted samples of future projections using Eq. (14) and (16), and simply subtract projection reference period mean modeled value for each model. As in previous work (Olson et al., 2017), we use 100,000 samples for all experiments.

The overall algorithm for the method is illustrated in Figure 2. The method estimates model weights from calibration period observations, and has one fixed parameter f , quantifying model error. Larger f values lead to higher model errors, and as a result broader projections with higher coverage of the 90% posterior credible intervals. Unlike standard Bayesian analysis, we first tweak f to obtain approximately correct empirical coverage of the 90% posterior credible intervals during cross-validation. For the cross-validation, each model is selected as the “truth” one-at-a-time. Models are weighted using the output from the “true” model. The “true” model is then excluded from the model set, and the future weighted projections from the remaining models are compared to the output from the “true” model. Once f achieves approximately correct empirical coverage, the method is used for actual projections constrained by real observations. If there are many replicates (or regions) of the system, cross-validation can also be performed by splitting the calibration period into two subperiods. In step 1, observations during the first subperiod in each region/replicate can be used to assign replicate/region-specific weights. In step 2, observations during the second subperiod can test the empirical coverage of the posterior credible intervals. Here, however, we focus on the one-at-a-time cross-validation.

In the next section we describe several cross-validation experiments for our method and compare the performance of the method (which we call hereafter “trend+var”) with the method where all variability submodel weights are set to equal (termed hereafter “trend”).

3 Observation System Simulation Experiments to Test Method Skill

3.1 Overview of Observation System Simulation Experiments

To evaluate method performance, we carry out observation system simulation experiments with several simulated and observed datasets: (i) Atlantic meridional overturning circulation (AMOC) strength [Sv] from 13 global climate models (GCMs) (AMOC experiment), (ii) Korean summer mean maximum temperatures from 29 GCMs (Korea_temp), (iii) Korean temperatures with an extended calibration period (Korea_temp_long), (iv) winter East Sea surface temperatures (SSTs) (Winter SST Experiment), (v) temperature-based AMOC Index (temperature in northern North Atlantic “gyre” minus Northern Hemisphere temperature) from 13 GCMs (AMOCIndex), and (vi) the same as (v) but also considering information from climate observations (AMOCIndex_obs). We discuss each experiment in greater detail in the following subsections. The cases differ in terms of the calibration, projection, and projection reference periods (Table 1). In experiments involving model output only, each of the models is selected as “truth” one at time, and its output is used to weight the models. Then, during the validation period, the projected pdfs

“trend+var” ALGORITHM

INPUT: trend and fluctuations model output for each model i for calibration period x_i and Δx_i , variability summary statistics $\tilde{\theta}_{M,i}^V$, corresponding trend and fluctuations observations y and Δy , projection period model output $x_i^{(f)}$ and $\Delta x_i^{(f)}$, model means during projection reference period $\bar{x}_i^{(r)}$.

OUTPUT: probability distribution of a metric change Δ between the projection and the projection reference periods

```

while coverage of 90% posterior credible interval  $\approx$  90% do
  set  $f$  #Choose  $f$  by trial and error
  for  $i$  in 1: $k$  do #Perform one-at-a-time cross-validation; select each model as “truth”
    assign  $y^i$  to  $x_i$ 
    assign  $\Delta y^i$  to  $\Delta x_i$ 
    for  $j=1:k$  do
      find  $p(M_{V,j}|\Delta y^i)$  using Eq. 9
      find  $p(M_{T,j}|y'^i)$  using Eq. 7
      find  $p(M_j|y^i, \Delta y^i)$  using Eq. 13
    end do
    find  $p(\Delta|D^i) = \sum_{j \neq i} p(\Delta|M_j, D^i)p(M_j|D^i)$  #where  $D^i = (y^i, \Delta y^i)$ 
    compare the 90% credible interval of  $\Delta$  to  $\Delta_i = \bar{x}_i^{(f)} - \bar{x}_i^{(r)}$ 
  end do
end do
# Use calibrated  $f$  from the cross-validation, perform real projections
for  $i=1:k$  do
  find  $p(M_{V,i}|\Delta y)$  using Eq. 9
  find  $p(M_{T,i}|y')$  using Eq. 7
  find  $p(M_i|y, \Delta y)$  using Eq. 13
end do
find  $p(\Delta|D) = \sum_{i=1}^k p(\Delta|M_i, D)p(M_i|D)$ 

```

Figure 2: “trend+var” algorithm.

of changes using the remaining models are compared to the “true” model output. The set-up for the AMOCIndex_obs is slightly different: both calibration and validation periods have available instrumental observations. Here, instead of selecting each model output as pseudo-observations one-at-a-time, we simply use actual observations to both weight the climate models, and to evaluate the projections. All experiments are performed with both “trend” and “trend+var” methods. Both methods have been calibrated for each experiment to have approximately correct coverage (correct % of cases where the “truth” is outside the 90% posterior credible intervals) by

tweaking model error expansion factor f (Table 1). The calibrated values of f for the AMOCIndex experiments are also used for the corresponding AMOCIndex_obs experiments. We focus on the Winter_SST experiment here, however summary results for all experiments are also provided.

3.2 AMOC Experiment

For the AMOC experiment (Table 1), data extraction and processing largely follow Olson et al., (2017). The Climate Model Intercomparison Project phase 5 (CMIP5; Taylor et al. 2011) model output for this (and other) experiments has been obtained from the ESGF LLNL portal (ESGF LLNL, 2016). Future forecasts use the RCP8.5 emissions scenario (Moss et al., 2010). We use robust locally-weighted “lowess” regression (Cleveland, 1979) to smooth the models in the calibration period, and Theil-Sen slopes (Sen, 1968) – in the validation period. We set the “lowess” smoother span parameter to 0.8 during the smoothing. We use this span value because it appears effective at removing interdecadal variability. The smoothed model output is illustrated in Figure 3. Importantly, we see nonlinearities in the modeled trends. Previous variability weighting work does not account for such nonlinearities (Fan et al., 2017). During the trend weighting we use smoothed output as anomalies with respect to the entire calibration period. We use normalized (by the absolute AMOC) fluctuations to weight the variability models. Future projections use the “boot” variant of the method.

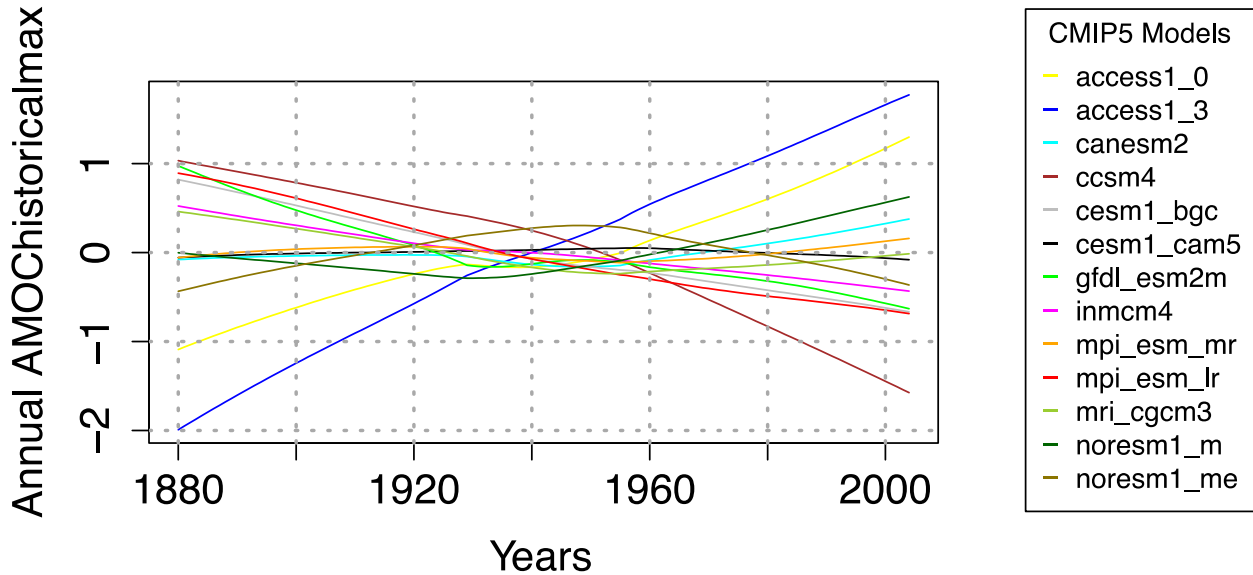


Figure 3: AMOC anomaly trends for the calibration period [Sv], as simulated by the CMIP5 climate models.

3.3 Korea_temp and Korea_temp_long Experiments

Korea_temp and Korea_temp_long differ only in the calibration periods and the error expansion factors f , with Korea_temp_long using a longer calibration period. These experiments use output from historical and future RCP8.5 runs of 29 CMIP5 model runs (Table 1, Table S1). First, Korean daily maximum temperatures are calculated as spatial averages over land grid cells

(cells with more than 80% land) between 34–40° N and 125–130° E (Shin et al., 2018). The JJA (June, July, August) means are then obtained for each year. Theil-Sen slopes are used for smoothing model output. During the weighting, smoothed output is used as anomalies with respect to the entire calibration period. Future projections use the “boot” variant of the method. Note that the Korea_temp “trend+var” experiment has a slightly elevated coverage of 93%. Decreasing f to obtain approximately 90% coverage is expected to improve performance metrics, but also to make probability densities too discontinuous. Hence, we use the value of $f=0.75$.

3.4 Winter_SST Experiment

Winter_SST experiment uses winter sea surface temperatures from the East Sea from historical and future RCP8.5 runs of 26 CMIP5 climate models (Table 1, Supplementary Table S2). We select this dataset because we find considerable relationships between present-day internal variability properties and future SST change in this region and season (Figure 4). We define the East Sea as an area between 35 °N and 42°N, and between 130 °E and 139 °E. We use a simple average of all ocean points in this region. During the weighting we use the output as anomalies with respect to the calibration period. Furthermore, we use Theil-Sen slopes to smooth the time series model output. Future projections use the “ar1” variant of the method, since we detect a considerable autocorrelation in the model output fluctuations.

3.5 AMOCIndex Experiment

AMOCIndex experiment (Table 1) relies on historical output from the same 13 CMIP5 models used for the AMOC experiment. AMOC Index is defined as sea surface temperature in northern North Atlantic “gyre” minus Northern Hemisphere temperature. It is physically linked to northward heat transport by the AMOC, and hence can be used as a proxy for AMOC (Olson et al., 2017; Rahmstorf et al., 2015). Data extraction and processing follow Olson et al. (2017), with a few changes. The Index is used as an anomaly with respect to the entire historical period 1880-2004. We then use a portion of the historical period (1880-1945) for calibration, and another portion (1965-2004) for projections. Smoothing is performed using Theil-Sen slopes. Projections use the “ar1” variant of the method.

3.6 AMOCIndex_obs Experiment

For the AMOCIndex_obs we use actual observations both to weight the models, and to validate the probabilistic projections. Otherwise, the experiment relies on the same model output as AMOCIndex experiment. The observations are a simple average of two AMOC Index versions: one calculated with ERSSTv4 SSTs (Huang et al., 2014, 2015; Liu et al., 2014), and one with COBE-SST2 SSTs (Hirahara et al., 2013). ERSSTv4 data is publicly curated by National Oceanic and Atmospheric Administration (Huang et al., 2016), while COBE-SST2 observations are provided by M. Ishii on the servers of Hokkaido University, Japan (Ishii, 2016). Both versions use GISTEMP Northern Hemisphere temperatures (Hansen et al., 2010). GISTEMP observations are maintained by NASA Goddard Institute for Space Studies (GISTEMP Team, 2016). For comparison with model output the COBE-SST2 SSTs are first interpolated to a $2\times 2^\circ$ grid using bilinear interpolation, while the ERSSTv4 observations are already on such a grid. For both “trend” and “trend+var” experiments, f is taken from corresponding AMOCIndex experiments.

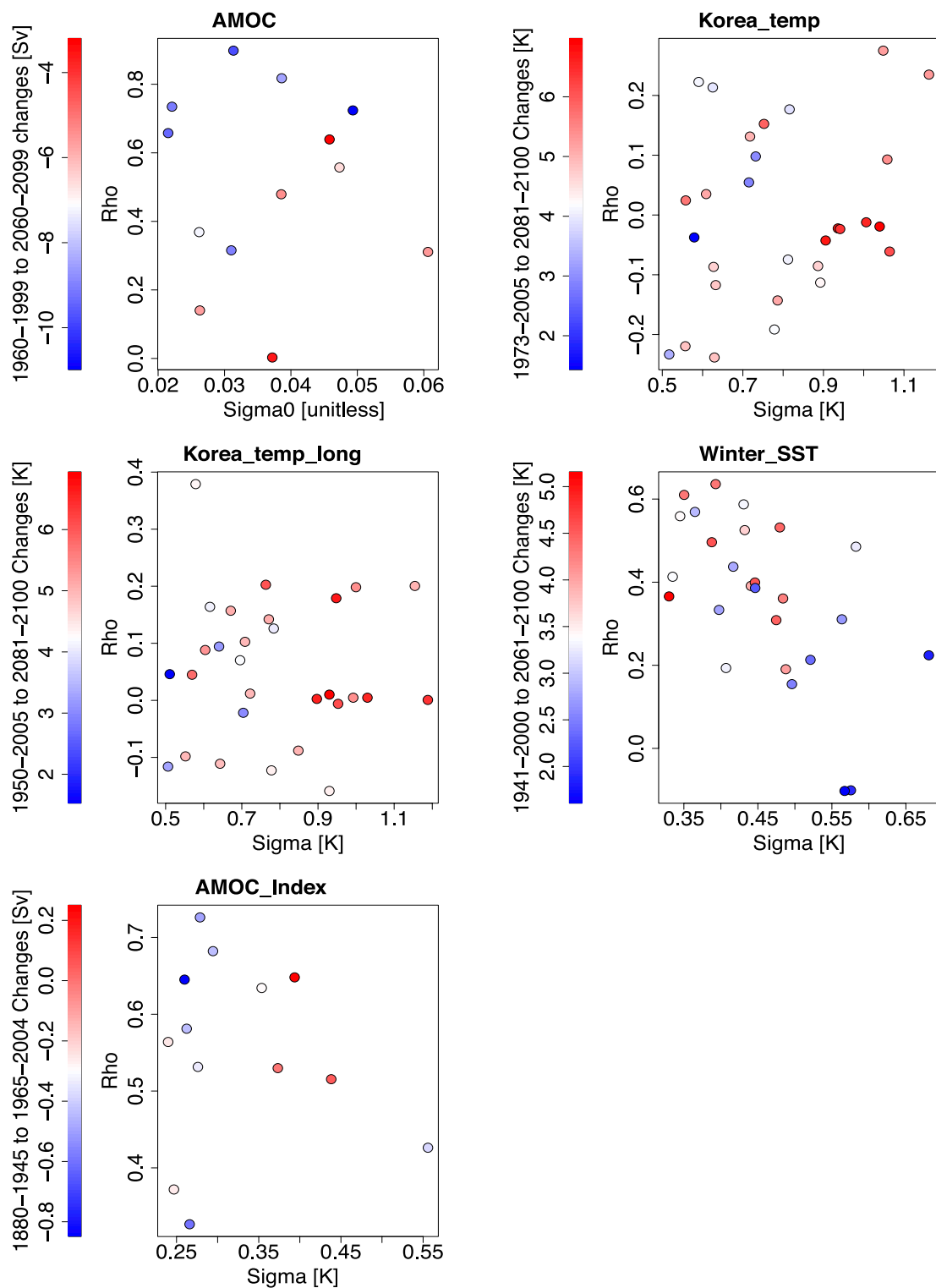


Figure 4. Relationship between sample innovation standard deviation (normalized in the AMOC experiment) and sample lag-1 autocorrelation of model fluctuations during the calibration, and projected changes (projected mean minus reference period mean) for the experiments using simulated data.

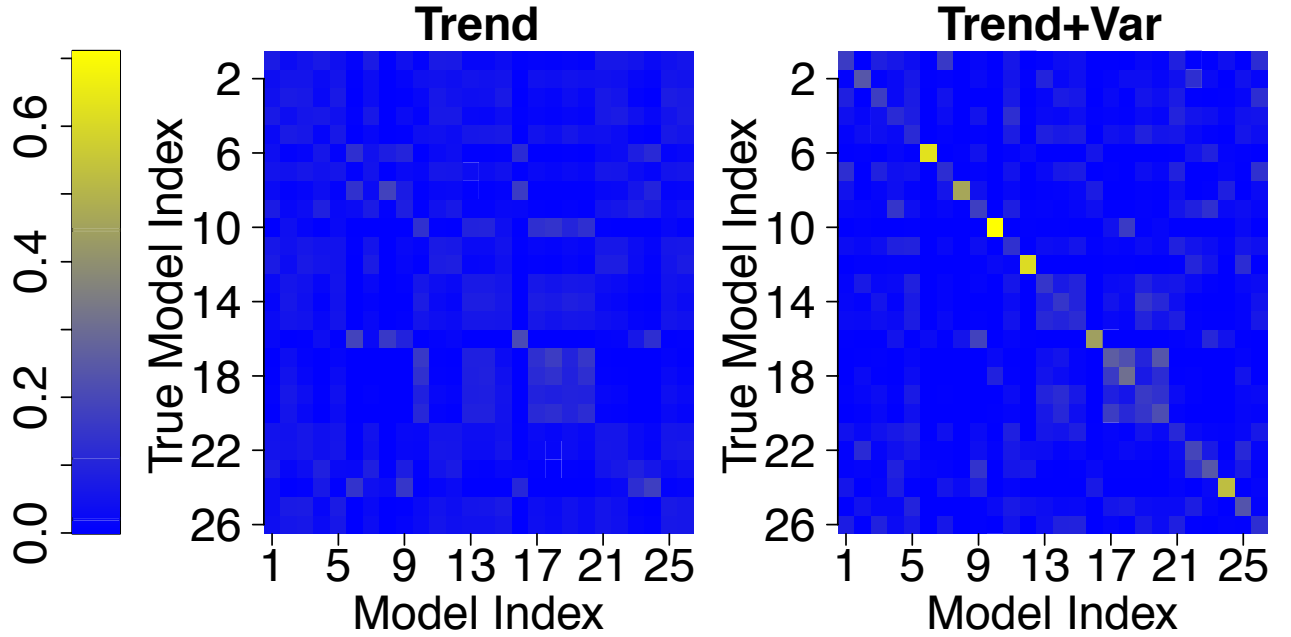


Figure 5. Model weights for Winter_SST cross-validation experiments. Rows represent different “true” models.

4 Results of Observation System Simulation Experiments

The new method tends to be better able to correctly identify the “true” model from pseudo-observations (Figure 5, Figure S12). This is not surprising since it uses extra fluctuations information that is not available to the “trend” method. This extra information can provide a powerful constraint because models differ considerably in their representation of internal variability, based on sample estimates of the variability properties (Figure 4). The most striking improvement is obtained for the AMOC experiment while arguably the least improvement – for the AMOCIndex (Figure S12).

Another important metric is the factor f that provides calibrated projections. This factor can be interpreted as a rough measure of model error relative to the next-closest inter-model differences in output space. The values feature a substantial range from 0.75 to 3.75 (Table 1). For experiments AMOC, AMOCIndex, and Korea_temp_long, f is the same or similar for both methods. Thus, under our statistical model, the best dynamical models for both “trend” and “trend+var” experiments are approximately equally close to the “true” unobserved trends in the real system, in both calibration and projection periods. However, for the rest of the simulated data experiments the new method achieves a lower f . Here, the best model for the “trend+var” method is closer (more than twice as close for Korea_temp) to the “true” trend of the system, compared to the best model under the “trend” experiment, both in calibration *and* projection periods.

We now turn our attention to the question of future prediction. First, it is worth noting that we do not find a significant bias between predicted and “true” projections in any of our one-at-a-time

observation system simulation experiments. The new method tends to improve in terms of the mean 90% credible interval width as well as mean absolute bias of the mean (Table 1, Figures 6, 7, S13-S16). Specifically, in the Korea_temp experiments, the forecast 90% credible intervals on average sharpen by about a quarter. For some cases (e.g., models 3 and 22 of the Korea_temp experiment), the improvements are particularly dramatic, featuring a drastic sharpening of the pdf and a strong reduction in the 90% credible intervals, with a low bias; Figures S15 and S16). The only cases with no improvement are AMOCIndex, and corresponding AMOCIndex_obs (Table 1). We note that these experiments rely on the same model output. They also use a weaker historical climate forcing during the projection period, whereas other experiments use stronger RCP8.5 future forcing. It is worthwhile noting that the experiments with the improvement boast a visual relationship between sample estimates of variability properties and future changes (Figure 4). Specifically, models with higher innovation standard deviation tend to produce higher summer mean maximum temperature warming in the Korean temperature experiments. A positive relationship between standard deviation and future temperature change have been previously found by Huttunen et al. (2017) for many regions. The relationships for the AMOC experiment are different: future AMOC slowdown appears to be stronger for models with higher autocorrelation and low normalized innovation standard deviation. In the Winter_SST experiment, the relationships also involve both variability properties: higher $\check{\sigma}_{M,i}$ and low $\check{\rho}_{M,i}$ in the models are associated with smallest future warming. The reasons for these relationships should be investigated in greater detail in future work. Thus, we speculate that the degree of improvement may be related to the strength of statistical relationships between the variability parameters and future change. Testing this hypothesis is left to future work. There can be considerable shifts in the pdf between the “trend” and “trend+var” method (Figures S13-S16). This is consistent with the fact that additional fluctuation data can provide a relatively independent constraint on the model weights.

We note that the improvement in performance by the “trend+var” method is not caused by any increase in number of parameters resulting in overfitting. The overall statistical model for the projections is the same in both cases: a weighted mixture of pdfs from individual models. The increase in skill is due to better estimation of individual model weights w_i in the “trend+var” model through using new variability data constraints on the models.

5 Real-Case Application: Projecting Korean Summer Mean Maximum Temperature

We now apply both the “trend” and “trend+var” methods to make projections of Korean summer mean maximum temperature. Specifically, we use 29 GCMs from Coupled Model Intercomparison Project phase 5 (CMIP5, Taylor et al., 2011) model runs (the same model set as for the Korea_temp experiment). The models are weighted using 1973-2005 station observational data provided by Korean Meteorological Administration (KMA) weather stations (Korea Meteorological Administration, 2016; Shin et al., 2018). We apply simple area average to daily mean maximum temperatures from the stations before calculating summer mean values. We use this short period because it has the best observational coverage, however to provide a liberal estimate of the uncertainty we take model error expansion factors f from the corresponding longer-period Korea_temp_long experiments. Future changes (2081-2100 minus 1973-2005) under the RCP8.5 emissions scenario (Moss et al., 2010) are presented in Figure 8. The results show (a)

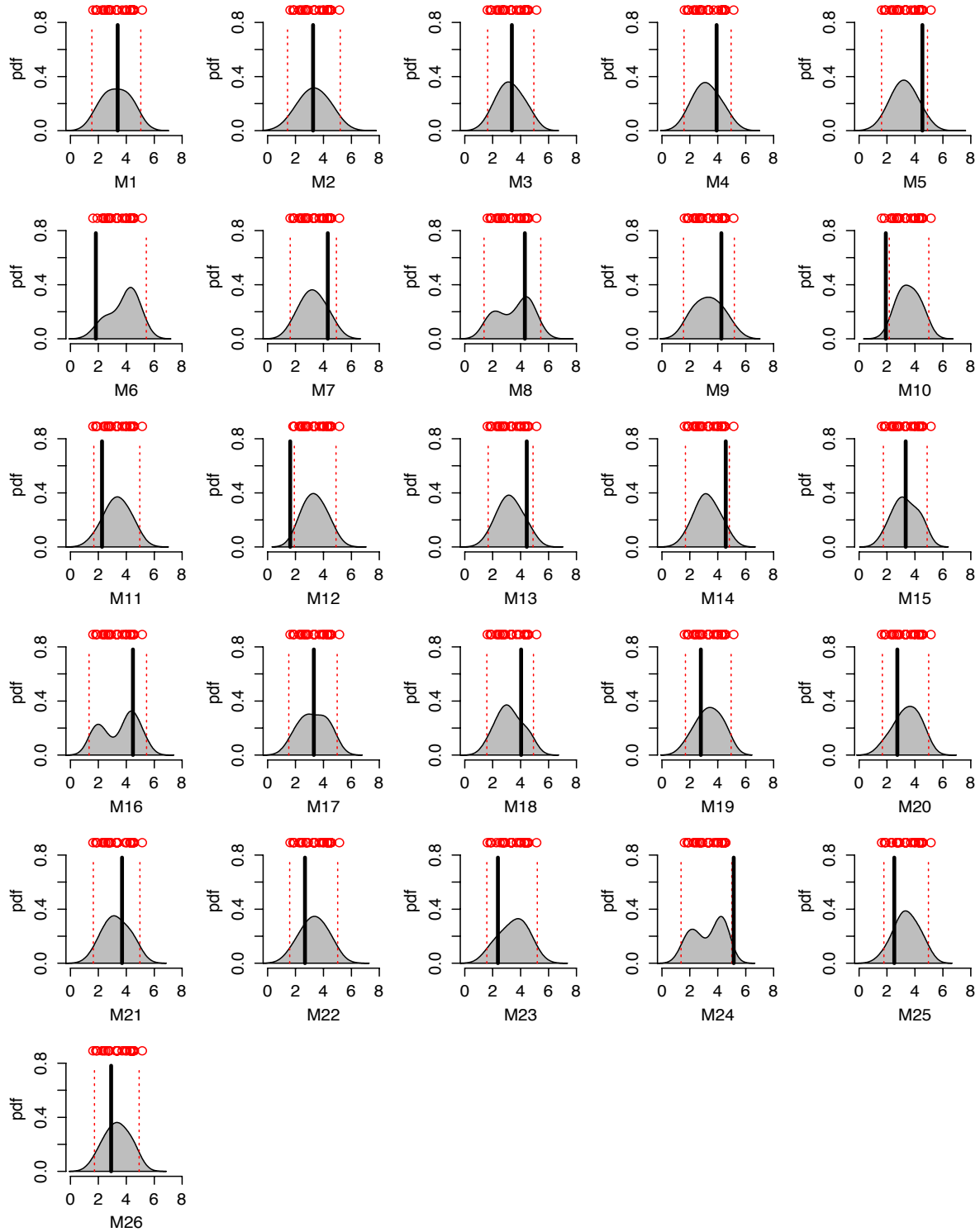


Figure 6. Probabilistic projections for winter East Sea surface temperature change from 1941-2000 to 2061-2100 [K] under the RCP8.5 emissions scenario for the “trend only” Winter_SST cross-validation experiment. Subplots differ in the assumed “true” model. Red circles are deterministic projections from each remaining model, red dotted lines are 90% posterior credible intervals. Black lines are changes from the “true” models.

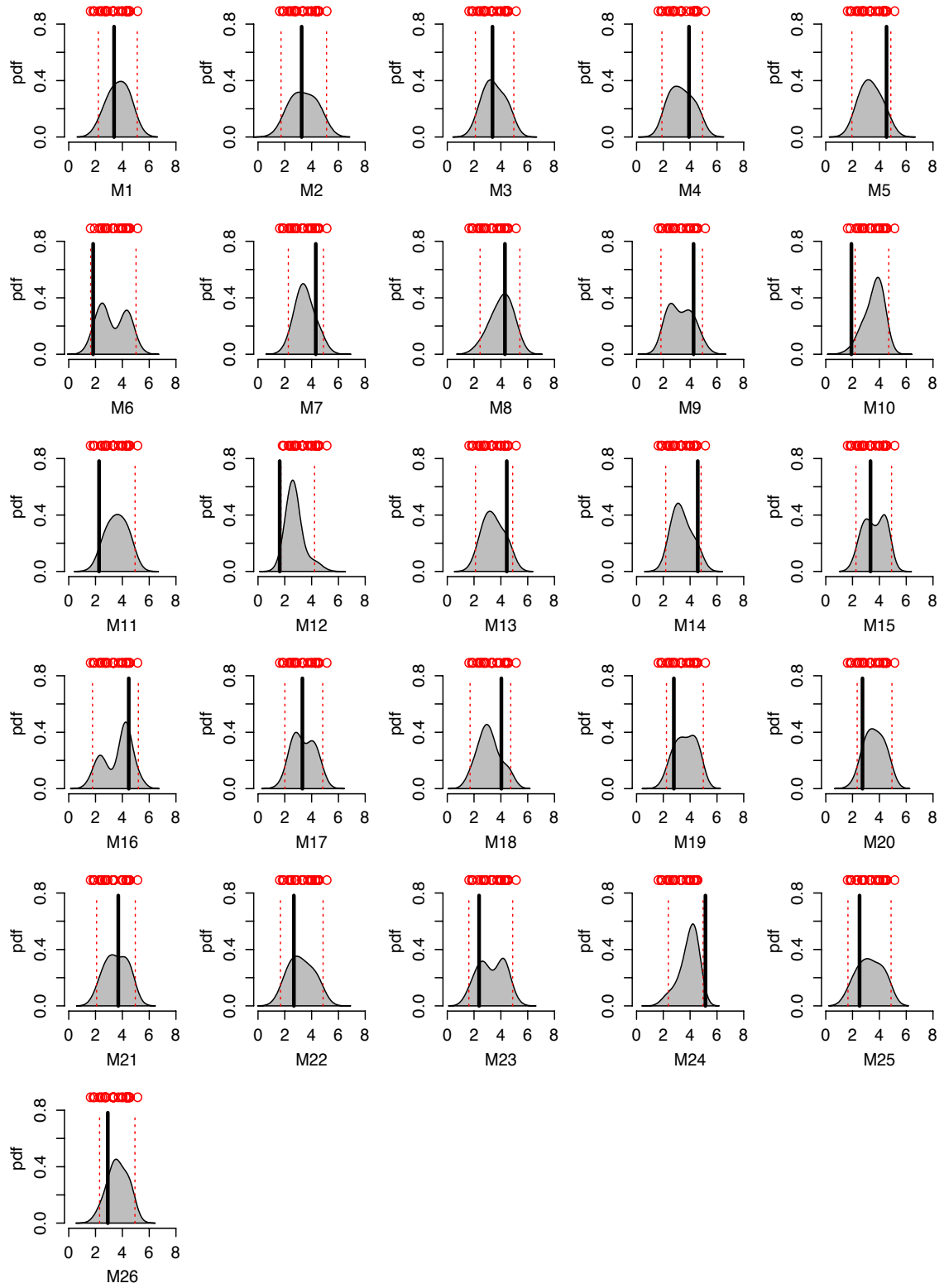


Figure 7. As Figure 6, but for “trend+var” experiment implementing the new proposed method

notably higher projected warming and (b) considerable reduction of the low-warming (< 2 K) tails after the variability weighting. Specifically, the mean increases from 4.9 K to 5.6 K, and the 5th percentile – from 1.8 K to 3.2 K. The new projection mode leaps from 5.3 K to 6.6 K (Table 2). In addition, the 90% credible interval shrinks from 5.5 K to 4.3 K (22 % reduction).

6 Discussion

Here we present a novel method “trend+var” to weight models of complex dynamical systems by their skill at representing both autocorrelated variability and the trend in observations. The key step is association of two statistical models with each dynamical model: a trend statistical model, and a variability statistical model. The component submodels are weighted separately using relevant observations, and then the weights are combined. The combined weights are used to make weighted probabilistic multi-model projections. In a series of observation system simulation experiments, we show that the new method appears to better identify the “true” model compared to the trend-only weighting method (“trend”). The new method also tends to perform better in terms of mean 90% posterior credible interval and mean absolute bias. Our analysis side-steps in some aspects from the traditional Bayesian framework, in order to avoid making difficult-to-justify parametric assumptions about model error, and to alleviate potential overconfidence in one-at-a-time cross-validation experiments.

Applying the new method to the real case of projecting Korean summer mean maximum temperature change by the end of this century considerably increases future projections. These projections are more informative than from the “trend” method because they use the additional variability and short-term memory (quantified by the lag-1 autocorrelation coefficient) information from both models and observations. Since the BMA predictive model is the same, the increase in skill is not due to an increased number of parameters, but is derived purely through better estimation of model weights. Recent work has found correlations with absolute values of up to approximately 0.8 between present-day interannual summer temperature sample standard deviation in global and regional climate models, and long-term future mean and/or variability changes for some regions (Fischer et al., 2012; Huttunen et al., 2017). This suggests that historical variability in those regions may provide a constraint on the models. Applying the method to those regions should be considered for future work.

It is worth discussing differences between this study and previous Bayesian work. Here we for the first time implement a quasi-Bayesian statistical method that weights models by their performance in terms of both trend, variability, and short-term memory (as quantified by the lag-1 autocorrelation) for a relatively general case: arbitrary non-linear trend function and red noise variability. The method can be extended to more complex variability structures. Model weights are obtained by constraining the method with calibration period observations, while a parameter controlling model error assumptions is calibrated using cross-validation experiments. Fan et al. (2017) also incorporate variability into model weights, however their method has so far been demonstrated on a simple case: serially uncorrelated variability, and a linear mean function. Other work (Buser et al., 2010; Chandler, 2013; Huttunen et al., 2017) also incorporates variability into the analyses. However, these studies do not actually use variability performance to weight the models and ignore autocorrelation skill. Unlike previous work, we do consider autocorrelation,

which is a common feature of variability in many observed and modeled processes (Hasselmann, 1976; Keller & McInerney, 2008; Olson et al., 2013).

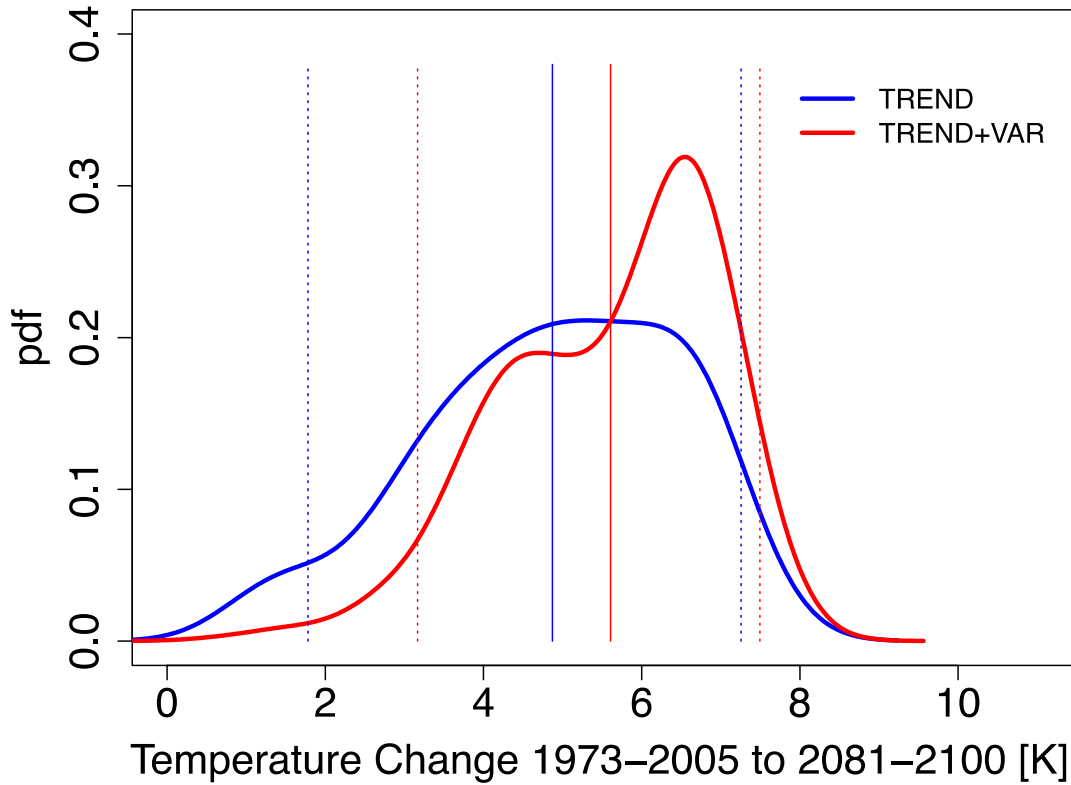


Figure 8. Probabilistic projections of summer mean maximum temperature change 1973-2005 to 2081-2100 over Korea under the RCP8.5 emissions scenario using “trend” and “trend+var” methods. Vertical lines are the means and the 90% posterior credible intervals.

7 Caveats

Our study is subject to several caveats. First, the fluctuations around the long-term trend, as well as model-observational residuals are assumed to be red noise processes. However, our framework can be extended to more general cases in the future. We compare the spectra of model fluctuations (normalized in the AMOC experiment) for each model and experiment to the 90% confidence intervals for the corresponding AR1 process spectra, based on 1000 random realizations (Figures S17-S19). Relevant comparison for the AMOCIndex experiment is shown in Figure 4 of Olson et al. (2017). These results indicate that AR1 process is a reasonable approximation to the internal variability for these systems. Second, when combining the weights

of the variability and trend submodels we are assuming independence. While this assumption appears to be generally reasonable here, it may not apply for other datasets. Incorporating dependence should be considered in future studies. Thus, our method is expected to be ideal for cases where there is at least some relationship between present-day variability and future changes, yet the relationship between present-day trends and variability in the models is sufficiently weak to justify the independence assumption we make here. Third, by using a common error expansion factor f for the internal variability, trend submodel errors, as well as for the forecasts, we are assuming the magnitudes of errors in these three components are linked. A way forward in subsequent work may be to assume different f for trend and variability. The best f values could then be found using constrained optimization (optimizing future performance metrics while constraining coverage to be correct). This is beyond the scope of this study. Fourth, when sampling future internal variability, we do not consider the uncertainty in the AR1 parameters of the fluctuations. However, as explained in Section 3, we calibrate our method to account for potential overconfidence by scaling the magnitude of the model errors. Other caveats include the simplicity of the future model bias and of the observation system simulation experiments, as well as no explicit representation of observational error. For the future Korean temperature projections, the high density of observational network mitigates some of these concerns, as random errors are expected to decrease after averaging across many stations. In addition, theoretically if modelled and observed data from multiple regions are used together in a cross-validation framework, the observational error will be implicitly incorporated into the analysis after nudging the f parameter. Nonetheless, an explicit representation of observed error should be considered in the future.

Notably, this work does not properly confront the issue of model dependence (e.g., the fact that models coming from the same research group, or models with similar outputs are dependent in the general sense of the term) (Annan and Hargreaves, 2017; Bishop and Abramowitz, 2012; Haughton et al., 2015; Leduc et al., 2016; Steinschneider et al., 2015 and others). This is addressed in a separate manuscript in review.

The best new datasets to apply the method to are the ones either with many regions, or with repeated experiments, and where a long calibration period can be split into two subperiods. In this case method performance can be systematically assessed using real observations in cross-validation experiments, and f can be properly calibrated. However, any assumption about f under new conditions is inherently untestable. Hence, we recommend including equal weights projections along with projections from this (or any other) weighting scheme. In the absence of many regions, and with only short time series available, one has to resort to simulated cross-validation experiments using calibration, projection, and projection reference period model output to calibrate the method. In such cases, if models share common errors, the real value of f may be higher than estimated.

8 Conclusions

We present a statistically-rigorous novel method to weight multiple models of stochastic dynamical systems by their skill at representing both internal variability (including autocorrelation) and a nonlinear trend of a time series process, and to make predictions of system change under new conditions. The weight is interpreted as a likelihood of a dynamical model being adequate at capturing both trend and variability aspects of the process. This is a particularly important diagnostic given the broad relevance of variability (e.g., variability can affect extreme events such as heat waves and droughts in climate science). We show that the proposed method tends to better

identify “true” models in a suite of observation system simulation experiments compared to the trend-only weighting method. The new method also tends to improve forecasts, as judged by the mean 90% credible interval width and mean absolute bias. This has important implications specifically for multi-model climate projections. Applying the method to project Korean summer mean maximum temperature changes over this century considerably increases future projections. Specifically, the mode of 1973-2005 to 2081-2100 warming under the RCP8.5 emissions scenario increases by 1.3 K to 6.6 K, while the mean shifts from 4.9 K to 5.6 K. Furthermore, the pdf becomes 22% sharper as measured by the 90% posterior credible interval.

Data and Software Availability

The data used are listed in the references. All R language code used to perform the statistical analysis and to produce the figures is available from the authors upon request.

Acknowledgments

For their roles in producing, coordinating, and making available the CMIP5 model output, we acknowledge the climate modeling groups, the World Climate Research Programme's (WCRP) Working Group on Coupled Modelling (WGCM), and the Global Organization for Earth System Science Portals (GO-ESSP). A portion of model outputs used here has been obtained from the German Climate Computing Centre (DKRZ), funded through the Federal Ministry for Education and Research. Jong-Soo Shin provided technical assistance with extracting Korean and East Sea temperature model output. "RO, and SA were supported by Basic Science Research Program through National Research Foundation of Korea (NRF-2017K1A3A7A03087790)". We are thankful to Cameron Farnsworth for providing comments on the manuscript, and to Soong-Ki Kim for thought-provoking discussions.

References

1. Acharya, N., Chattopadhyay, S., Mohanty, U. C., & Ghosh, K. (2014). Prediction of Indian summer monsoon rainfall: a weighted multi-model ensemble to enhance probabilistic forecast skills. *Meteorol. Appl.*, 21(3), 724–732. <https://doi.org/10.1002/met.1400>
2. Annan, J. D. & Hargreaves, J. C. (2017). On the meaning of independence in climate science. *Earth Syst. Dyn.*, 8(1), 211–224 (2017). <https://doi.org/10.5194/esd-8-211-2017>
3. Bayes, M., & Price, M. (1763). An Essay towards Solving a Problem in the Doctrine of Chances. By the Late Rev. Mr. Bayes, F. R. S. Communicated by Mr. Price, in a Letter to John Canton, A. M. F. R. S. *Philos. Trans.*, 53, 370–418. <https://doi.org/10.1098/rstl.1763.0053>
4. Bhat, K. S., Haran, M., Terando, A., & Keller, K. (2011). Climate Projections Using Bayesian Model Averaging and Space-Time Dependence. *J. Agric. Biol. Environ. Stat.*, 16(4), 606–628. <https://doi.org/10.1007/s13253-011-0069-3>
5. Bishop, C. H. & Abramowitz, G. (2012). Climate model dependence and the replicate Earth paradigm. *Clim. Dyn.*, 41(3-4), 885–900. <https://doi.org/10.1007/s00382-012-1610-y>

6. Braverman, A., Cressie, N., & Teixeira, J. (2011). A likelihood-based comparison of temporal models for physical processes. *Stat. Anal. Data Min.*, 4(3), 247–258. <https://doi.org/10.1002/sam.10113>
7. Buser, C. M., Künsch, H. R., & Schär, C. (2010). Bayesian multi-model projections of climate: Generalization and application to ENSEMBLES results. *Clim. Res.*, 44(2–3), 227–241. <https://doi.org/10.3354/cr00895>
8. Buser, C. M., Künsch, H. R., Lüthi, D., Wild, M., & Schär, C. (2009). Bayesian multi-model projection of climate: bias assumptions and interannual variability. *Clim. Dyn.*, 33(6), 849–868. <https://doi.org/10.1007/s00382-009-0588-6>
9. Chandler, R. E. (2013). Exploiting strength, discounting weakness: combining information from climate simulators. *Philos. Trans. R. Soc. Lond. Ser. A*, 371, 20120388 multiple –20120388. <https://doi.org/10.1098/rsta.2012.0388>
10. Cleveland, W. S. (1979). Robust Locally Weighted Regression and Smoothing Scatterplots. *J. Am. Stat. Assoc.*, 74(368), 829–836. <https://doi.org/10.1080/01621459.1979.10481038>
11. Cox, P. M., C. Huntingford, and M. S. Williamson (2018). Emergent constraint on equilibrium climate sensitivity from global temperature variability. *Nat.*, 553, pp. 319–322. <https://doi.org/10.1038/nature25450>
12. Duan, Q., Ajami, N. K., Gao, X., & Sorooshian, S. (2007). Multi-model ensemble hydrologic prediction using Bayesian model averaging. *Adv. Water Resour.*, 30(5), 1371–1386. <https://doi.org/10.1016/j.advwatres.2006.11.014>
13. [dataset] ESGF LLNL. (2016). ESGF @ DOE/LLNL. Retrieved from <https://esgf-node.llnl.gov/projects/esgf-llnl/>
14. Fan, Y., Olson, R., & Evans, J. P. (2017). A Bayesian posterior predictive framework for weighting ensemble regional climate models. *Geosci. Model Dev.*, 10(6), 2321–2332. <https://doi.org/10.5194/gmd-10-2321-2017>
15. Feng Q. Y., Viebahn J. P., & Dijkstra H. A. (2014). Deep ocean early warning signals of an Atlantic MOC collapse. *Geophys. Res. Lett.*, 41(16), 6008–6014. <https://doi.org/10.1002/2014GL061019>
16. Fischer, E. M., Rajczak, J., & Schär, C. (2012). Changes in European summer temperature variability revisited. *Geophys. Res. Lett.*, 39(19), L19702. <https://doi.org/10.1029/2012GL052730>
17. [dataset] GISTEMP Team. (2016). GISS Surface Temperature Analysis (GISTEMP). NASA Goddard Institute for Space Studies. Retrieved from <https://data.giss.nasa.gov/gistemp/>
18. Hansen, J., Ruedy, R., Sato, M., & Lo, K. (2010). Global Surface Temperature Change. *Rev. Geophys.*, 48(4), RG4004. <https://doi.org/10.1029/2010RG000345>
19. Hasselmann, K. (1976). Stochastic climate models Part I. Theory. *Tellus*, 28(6), 473–485. <https://doi.org/10.3402/tellusa.v28i6.11316>
20. Haughton, N., Abramowitz, G., Pitman, A. & Phipps, S. J. (2015). Weighting climate model ensembles for mean and variance estimates. *Clim. Dyn.*, 45(11–12), 3169–3181. <https://doi.org/10.1007/s00382-015-2531-3>
21. Hirahara, S., Ishii, M., & Fukuda, Y. (2013). Centennial-Scale Sea Surface Temperature Analysis and Its Uncertainty. *J. Clim.*, 27(1), 57–75. <https://doi.org/10.1175/JCLI-D-12-00837.1>

22. Hoeting, J. A., Madigan, D., Raftery, A. E., & Volinsky, C. T. (1999). Bayesian Model Averaging: A Tutorial. *Stat. Sci.*, 14(4), 382–417.
23. Huang, B., Thorne, P. W., Smith, T. M., Liu, W., Lawrimore, J., Banzon, V. F., Zhang, H.-M., Peterson, T. C., & Menne, M. (2015). Further Exploring and Quantifying Uncertainties for Extended Reconstructed Sea Surface Temperature (ERSST) Version 4 (v4). *J. Clim.*, 29(9), 3119–3142. <https://doi.org/10.1175/JCLI-D-15-0430.1>
24. Huang, B., Banzon, V. F., Freeman, E., Lawrimore, J., Liu, W., Peterson, T. C., Smith, T. M., Thorne, P. W., Woodruff, S. D., & Zhang, H.-M. (2014). Extended Reconstructed Sea Surface Temperature Version 4 (ERSST.v4). Part I: Upgrades and Intercomparisons. *J. Clim.*, 28(3), 911–930. <https://doi.org/10.1175/JCLI-D-14-00006.1>
25. [dataset] Huang, B., Banzon, V. F., Freeman, E., Lawrimore, J., Liu, W., Peterson, T. C., Smith, T. M., Thorne, P. W., Woodruff, S. D., & Zhang, H.-M. (2016). Extended Reconstructed Sea Surface Temperature (ERSST), Version 4, NOAA National Centers for Environmental Information. Retrieved from <https://data.nodc.noaa.gov/cgi-bin/iso?id=gov.noaa.ncdc:C00884>, doi:10.7289/V5KD1VVF
26. Huttunen, J. M. J., Räisänen, J., Nissinen, A., Lipponen, A., & Kolehmainen, V. (2017). Cross-validation analysis of bias models in Bayesian multi-model projections of climate. *Clim. Dyn.*, 48(5–6), 1555–1570. <https://doi.org/10.1007/s00382-016-3160-1>
27. [dataset] Ishii, M. (2016). COBE-SST2 Version 2.9.2. Retrieved from <https://amaterasu.ees.hokudai.ac.jp/~ism/pub/cobe-sst2/>
28. Keller, K., & McInerney, D. (2008). The dynamics of learning about a climate threshold. *Clim. Dyn.*, 30(2–3), 321–332. <https://doi.org/10.1007/s00382-007-0290-5>
29. Kleinen, T., Held, H., & Petschel-Held, G. (2003). The potential role of spectral properties in detecting thresholds in the Earth system: Application to the thermohaline circulation. *Ocean Dyn.*, 53(2), 53–63. <https://doi.org/10.1007/s10236-002-0023-6>
30. Knutti, R. (2008). Should we believe model predictions of future climate change? *Philos. Trans. R. Soc. Lond. Ser. A: Math., Phys. Eng. Sci.*, 366(1885), 4647–4664. <https://doi.org/10.1098/rsta.2008.0169>
31. Kopp, R. E., Shwom, R. L., Wagner, G., & Yuan, J. (2016). Tipping elements and climate-economic shocks: pathways towards integrated assessment. *Earth's Future*, 4, 346–372.
32. [dataset] Korea Meteorological Administration. (2016). Open Portal for Meteorological Data (in Korean). Retrieved from <https://data.kma.go.kr>
33. Kwasniok, F. (2013). Analysis and modelling of glacial climate transitions using simple dynamical systems. *Phil. Trans. R. Soc. A*, 371(1991), 20110472. <https://doi.org/10.1098/rsta.2011.0472>
34. Leduc, M., Laprise, R., de Elía, R., & Šeparović, L (2016). Is Institutional Democracy a Good Proxy for Model Independence? *J. Clim.*, 29(23), 8301–8316. <https://doi.org/10.1175/JCLI-D-15-0761.1>
35. Lenton, T. M., Livina, V. N., Dakos, V., Van Nes, E. H., & Scheffer, M. (2012). Early warning of climate tipping points from critical slowing down: comparing methods to improve robustness. *Philos. T. R. Soc. A.*, 370(1962), 1185–1204, <https://doi.org/10.1098/rsta.2011.0304>
36. Liu, W., Huang, B., Thorne, P. W., Banzon, V. F., Zhang, H.-M., Freeman, E., Lawrimore, J., Peterson, T. C., Smith, T. M., & Woodruff, S. D. (2014). Extended Reconstructed Sea Surface Temperature Version 4 (ERSST.v4): Part II. Parametric and

- Structural Uncertainty Estimations. *J. Clim.*, 28(3), 931–951.
<https://doi.org/10.1175/JCLI-D-14-00007.1>
37. Montgomery, J. M., & Nyhan, B. (2010). Bayesian model averaging: Theoretical developments and practical applications. *Political Anal.*, 18(2), 245–270.
<https://doi.org/10.1093/pan/mpq001>
 38. Moss, R. H., Edmonds, J. A., Hibbard, K. A., Manning, M. R., Rose, S. K., van Vuuren, D. P., Carter, T. R., Emori, S., Kainuma, M., Kram, T., Meehl, G. A., Mitchell, J. F. B., Nakicenovic, N., Riahi, K., Smith, S. J., Stouffer, R. J., Thomson, A. M., Weyant, J. P., & Wilbanks, T. J. (2010). The next generation of scenarios for climate change research and assessment. *Nat.*, 463(7282), 747–756. <https://doi.org/10.1038/nature08823>
 39. Olson, R., An, S.-I., Fan, Y., Evans, J. P., & Caesar, L. (2017). North Atlantic observations sharpen meridional overturning projections. *Clim. Dyn.*, 1–18.
<https://doi.org/10.1007/s00382-017-3867-7>
 40. Olson, R., Fan, Y., & Evans, J. P. (2016). A simple method for Bayesian model averaging of regional climate model projections: Application to southeast Australian temperatures. *Geophys. Res. Lett.*, 43(14), 2016GL069704.
<https://doi.org/10.1002/2016GL069704>
 41. Olson, R., Srivier, R., Chang, W., Haran, M., Urban, N. M., & Keller, K. (2013). What is the effect of unresolved internal climate variability on climate sensitivity estimates? *J. Geophys. Res. Atmos.*, 118(10), 4348–4358. <https://doi.org/10.1002/jgrd.50390>
 42. Peavoy, D., & Franzke, C. (2010). Bayesian analysis of rapid climate change during the last glacial using Greenland $\delta^{18}\text{O}$ data. *Clim. Past*, 6(6), 787–794.
<https://doi.org/10.5194/cp-6-787-2010>
 43. Qi, Y., Qian, C., & Yan, Z. (2017). An alternative multi-model ensemble mean approach for near-term projection. *Int. J. Clim.*, 37(1), 109–122. <https://doi.org/10.1002/joc.4690>
 44. Rahmstorf, S., Box, J. E., Feulner, G., Mann, M. E., Robinson, A., Rutherford, S., and Schaffernicht, E. J. (2015). Exceptional twentieth-century slowdown in Atlantic Ocean overturning circulation. *Nat. Clim. Chang.*, 5(5), 475–480. doi: 10.1038/nclimate2554
 45. Raftery, A. E., Gneiting, T., Balabdaoui, F., & Polakowski, M. (2005). Using Bayesian model averaging to calibrate forecast ensembles. *Mon. Weather Rev.*, 133(5), 1155–1174.
<https://doi.org/10.1175/MWR2906.1>
 46. Rougier, J., Goldstein, M., & House, L. (2013). Second-order exchangeability analysis for multimodel ensembles. *J. Am. Stat. Assoc.*, 108(503), 852–863.
<https://doi.org/10.1080/01621459.2013.802963>
 47. Sen, P. K. (1968). Estimates of the Regression Coefficient Based on Kendall's Tau. *J. Am. Stat. Assoc.*, 63(324), 1379–1389. <https://doi.org/10.2307/2285891>
 48. Sexton D. M. H., Murphy J. M., Collins M., & Webb M. J. (2011). Multivariate probabilistic projections using imperfect climate models part I: outline of methodology. *Clim. Dyn.*, 38, 2513–2542. doi: 10.1007/s00382-011-1208-9
 49. Shin, J., Olson, R., & An, S.-I. (2018). Projected Heat Wave Characteristics over the Korean Peninsula During the Twenty-First Century. *Asia-Pacific J. Atmos. Sci.* 54(1), 53–61. <https://doi.org/10.1007/s13143-017-0059-7>
 50. Steinschneider, S., McCrary, R., Mearns, L. O., & Brown, C. (2015). The effects of climate model similarity on probabilistic climate projections and the implications for local, risk-based adaptation planning. *Geophys. Res. Lett.*, 42(12), 2015GL064529.
<https://doi.org/10.1002/2015GL064529>

51. Taylor, K. E., Stouffer, R. J., & Meehl, G. A. (2011). An Overview of CMIP5 and the Experiment Design. *Bull. Am. Meteorol. Soc.*, 93(4), 485–498. <https://doi.org/10.1175/BAMS-D-11-00094.1>
52. Tebaldi, C., Sanso, B., Smith, R. L., & Ferreira, M. A. R. (2011). Characterizing Uncertainty of Future Climate Change Projections using Hierarchical Bayesian Models. In Jose Bernardo, M. J. Bayarri, J. O. Berger, A. P. Dawid, D. Heckerman, A. F. M. Smith, & M. West (Eds.), *Bayesian Statistics 9*. Oxford Scholarship Online.
53. Tebaldi, C., & Sansó, B. (2009). Joint projections of temperature and precipitation change from multiple climate models: A hierarchical Bayesian approach. *J. R. Stat. Soc. Ser. A: Stat. Soc.*, 172(1), 83–106. <https://doi.org/10.1111/j.1467-985X.2008.00545.x>
54. Terando, A., Keller, K., & Easterling, W. E. (2012). Probabilistic projections of agro-climate indices in North America. *J. Geophys. Res. Atmos.*, 117(8). <https://doi.org/10.1029/2012JD017436>
55. Thomas, Z. A. (2016). Using natural archives to detect climate and environmental tipping points in the Earth System. *Quat. Sci. Rev.*, 152, 60–71. <https://doi.org/10.1016/j.quascirev.2016.09.026>
56. Wallach, D., Mearns, L. O., Ruane, A. C., Rötter, R. P., & Asseng, S. (2016). Lessons from climate modeling on the design and use of ensembles for crop modeling. *Clim. Chang.*, 139(3–4), 551–564. <https://doi.org/10.1007/s10584-016-1803-1>
57. Xu, Y., Gao, X., & Giorgi, F. (2010). Upgrades to the reliability ensemble averaging method for producing probabilistic climate-change projections. *Clim. Res.*, 41(1), 61–81. <https://doi.org/10.3354/cr00835>
58. Yun, W. T., Stefanova, L., & Krishnamurti, T. N. (2003). Improvement of the Multimodel Superensemble Technique for Seasonal Forecasts. *J. Clim.*, 16(22), 3834–3840. [https://doi.org/10.1175/1520-0442\(2003\)016<3834:IOTMST>2.0.CO;2](https://doi.org/10.1175/1520-0442(2003)016<3834:IOTMST>2.0.CO;2)
59. Yun, W. T., Stefanova, L., Mitra, A. K., Kumar, T. S. V. V., Dewar, W., & Krishnamurti, T. N. (2005). A multi-model superensemble algorithm for seasonal climate prediction using DEMETER forecasts. *Tellus A*, 57(3), 280–289. <https://doi.org/10.1111/j.1600-0870.2005.00131.x>

Tables

Experiment	k ¹	Calibration Period	Projection Reference Period	Projection Period	Trend f	Trend +Var f	Metric	Trend	Trend+Var
AMOC	13	1880-2004	1960-1999	2060-2099	1.5	1.5	MCIW ²	9.53 Sv	9.46 Sv
							MAB ³	2.30 Sv	2.06 Sv
Korea_temp	29	1973-2005	1973-2005	2081-2100	1.55	0.75	MCIW	4.34 K	3.23 K
							MAB	1.01 K	0.88 K
Korea_temp_long	29	1950-2005	1950-2005	2081-2100	2.22	2.3	MCIW	4.28 K	3.60 K
							MAB	0.96 K	0.79 K
Winter_SST	26	1941-2000	1941-2000	2061-2000	2.5	2.05	MCIW	3.40 K	2.90 K
							MAB	0.86 K	0.78 K
AMOCIndex	13	1880-1945	1880-1945	1965-2004	3.75	3.75	MCIW	1.42 K	1.44 K
							MAB	0.23 K	0.23 K
AMOCIndex_obs	13	1880-1945	1880-1945	1965-2004	3.75	3.75	CIW ⁴	1.42 K	1.43 K
							AB ⁵	0.42 K	0.41 K

Table 1. Basic information about the design of observation system simulation experiments, and the method performance. **Bold font** indicates improvement on the “trend” method

¹The number of models in the ensemble

5

²Mean 90% credible interval width

³Mean absolute bias of the mean

⁴90% credible interval width

⁵Absolute bias of the mean.

Experiment	Mean	Median	Mode	90% Credible Interval
Trend	4.9 K	5.0 K	5.3 K	(1.8, 7.3)
Trend+var	5.6 K	5.9 K	6.6 K	(3.2, 7.5)

Table 2. Summary of Korean summer mean maximum temperature probabilistic projections 1973-2005 to 2081-2100 under the RCP8.5 emissions scenario from the “trend” and “trend+var” methods

Supporting Information for “Accounting for Skill in Nonlinear Trend, Variability, and Autocorrelation Facilitates Better Multi-Model Projections”

Roman Olson^{a,b,c}, Soon-Il An^a, Yanan Fan^d and Jason P. Evans^e

^aDepartment of Atmospheric Sciences, Yonsei University, Seoul, South Korea, 03722

^bCenter for Climate Physics, Institute for Basic Science, Busan, South Korea, 46241

^cPusan National University, Busan, South Korea, 46241

^dSchool of Mathematics and Statistics, UNSW, Sydney, NSW, 2052, Australia

^eClimate Change Research Centre and ARC Centre for Excellence in Climate Extremes,
UNSW Australia, Sydney, NSW, Australia

Contents of this file

Text S1 and S2
Figures S1 to S19
Tables S1 to S2

Introduction

Supporting Texts contains information on details of the statistical methodology. Text S1 provides technical details on weighting trend models, while Text S2 discusses the implementation of the variability model weighting.

Text S1.

For the Monte Carlo integration to get trend submodel weights, we use 100,000 samples for all experiments except “trend” Korea_temp, AMOCIndex and AMOCIndex_obs which use 1,000,000 samples. The real-case Korean temperature projections also use 1,000,000 samples. When we repeat Korea_temp experiments with a different number of samples (1,000,000 for “trend+var” and 100,000 for “trend”), the performance metrics for these experiments are virtually identical. This suggests that 100,000 samples are enough to reasonably estimate method performance. We employ uniform priors for σ on $[0, 5]$, and for ρ on $[-1, 1]$ for the AR1 properties of the internal variability during the trend weighting in all experiments.

Text S2.

For the Monte Carlo integration to get variability submodel weights, we use 10,000 samples for all relevant experiments. The real-case Korean temperature projections use 100,000 samples. Since the results for the performance metrics are virtually identical for the longer Korea_temp “trend+var” experiment described in Text S1 (which uses 100,000 samples for variability weights estimation), we deduce that 10,000 samples is a reasonable number. When sampling θ_y^V we set autocorrelations with absolute values of 0.999 or higher to ± 0.999 for numerical stability reasons. Likewise, we restrict ourselves to positive innovation standard deviations by setting all values below $0.01 \times \min(\check{\sigma}_M)$ to $0.01 \times \min(\check{\sigma}_M)$. Here $\check{\sigma}_M$ is a vector of all standard deviation summary statistics from all dynamical variability models: $\check{\sigma}_M = (\check{\sigma}_{M,1}, \dots, \check{\sigma}_{M,k})$.

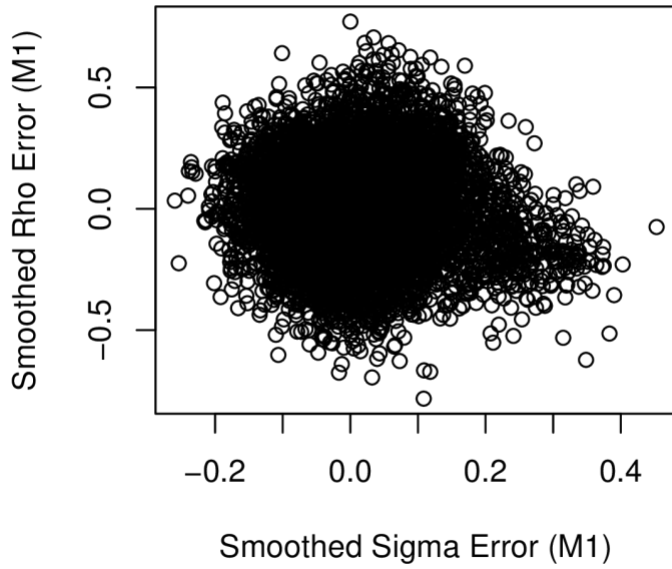
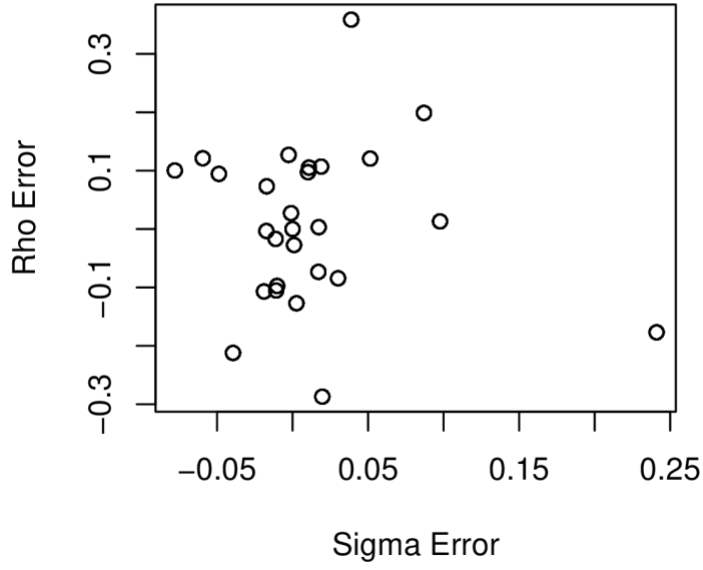


Figure S1. (top) 26 samples of $f\epsilon^V = f(\epsilon_\sigma, \epsilon_\rho)$ provided by next-closest model differences for the Winter_SST experiment, together with the (0,0) sample, (bottom) samples augmented by samples from the bivariate normal distribution with standard deviations set to 1/5 of the initial sample ranges, used in weighting the 1st variability model.

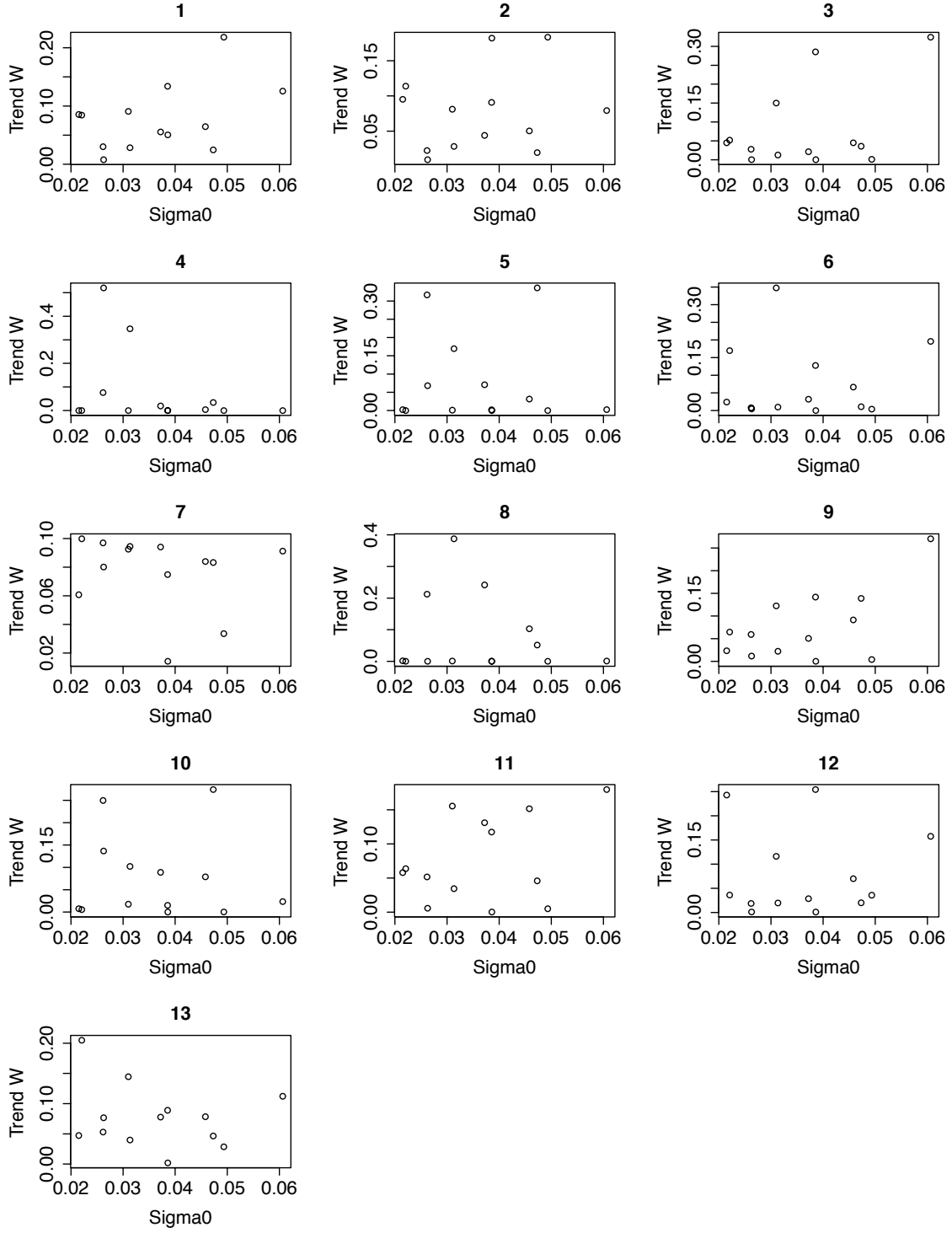


Figure S2. Correlation between normalized innovation standard deviation summary statistics and trend weights $p(M_{T,i})$ for the AMOC experiment. Each panel corresponds to a different “true” model used as pseudo-observations.

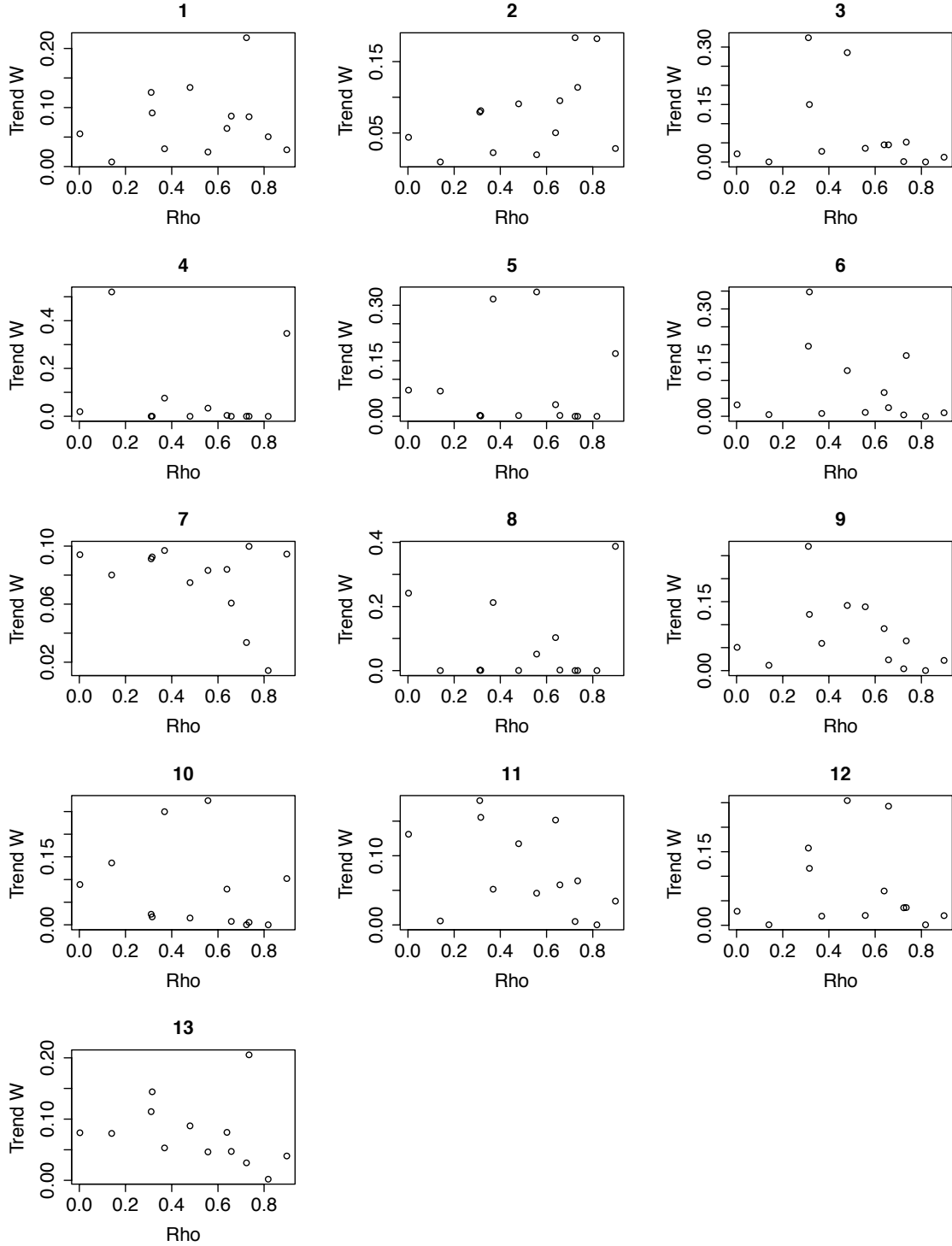


Figure S3. Correlation between autocorrelation summary statistics and trend weights $p(M_{T,i})$ for the AMOC experiment. Each panel corresponds to a different "true" model used as pseudo-observations.

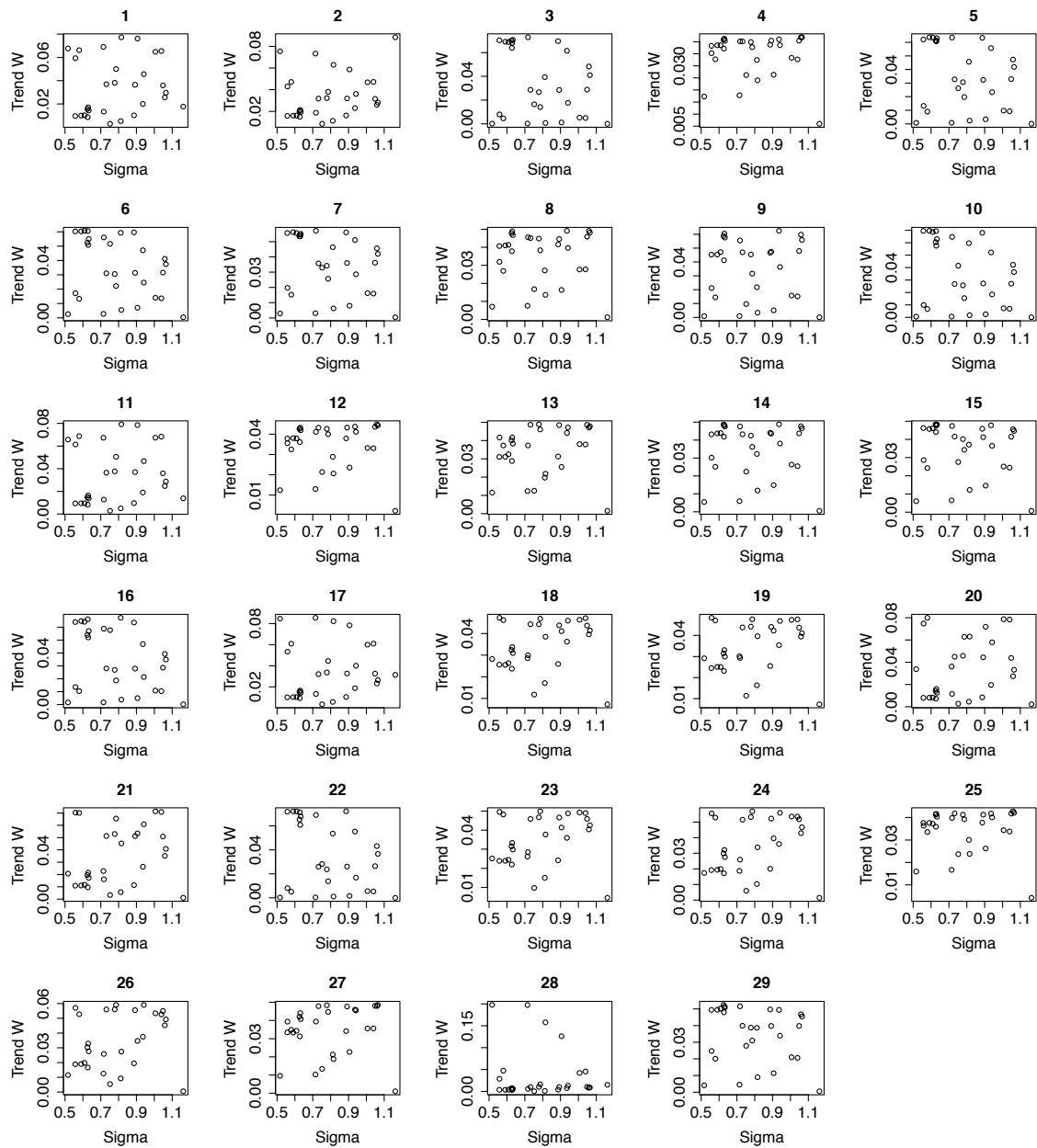


Figure S4. Same as Figure S2, but for un-normalized standard deviation [K] and the Korea_temp experiment.

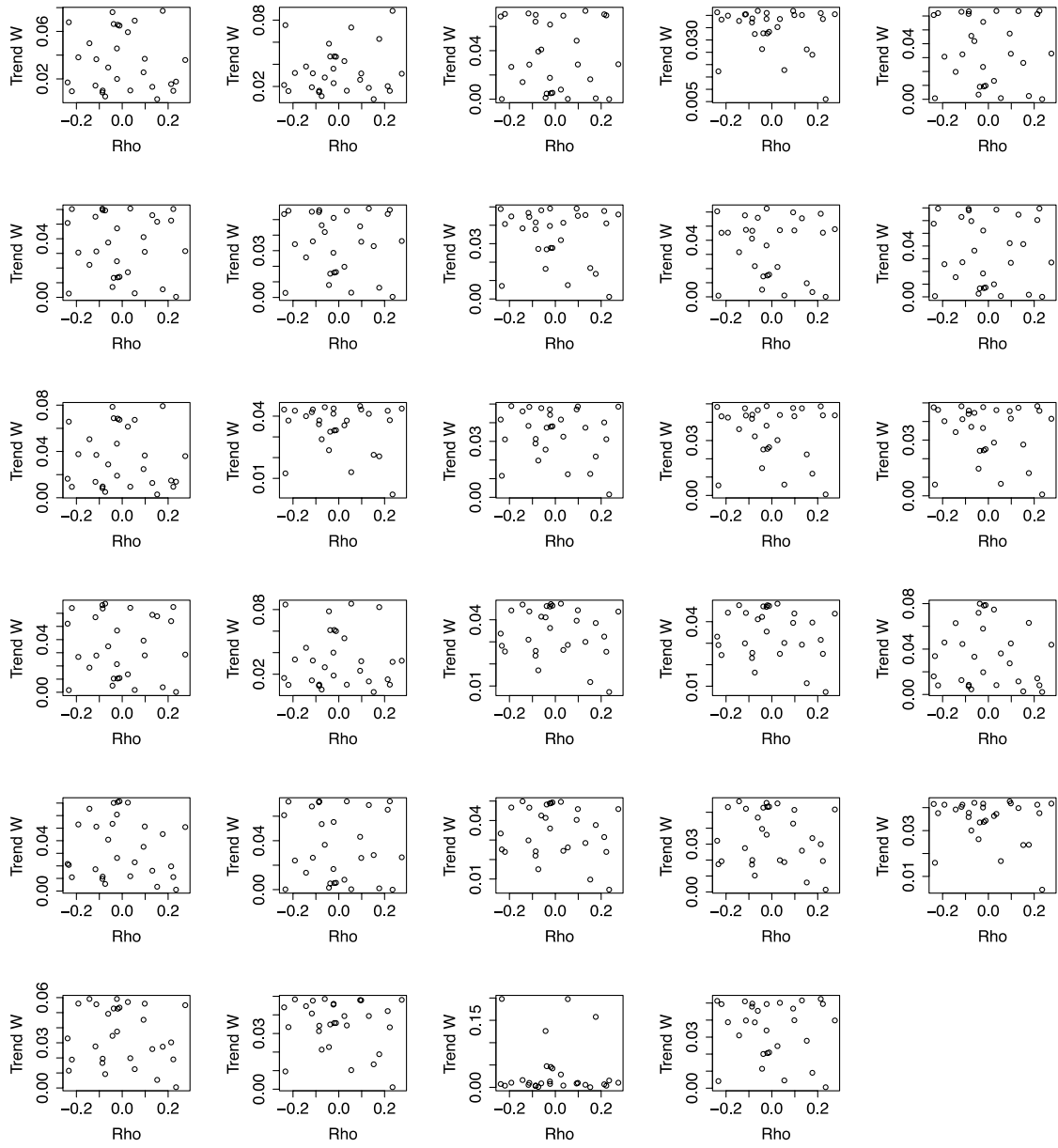


Figure S5. Same as Figure S3, but for the Korea_temp experiment.

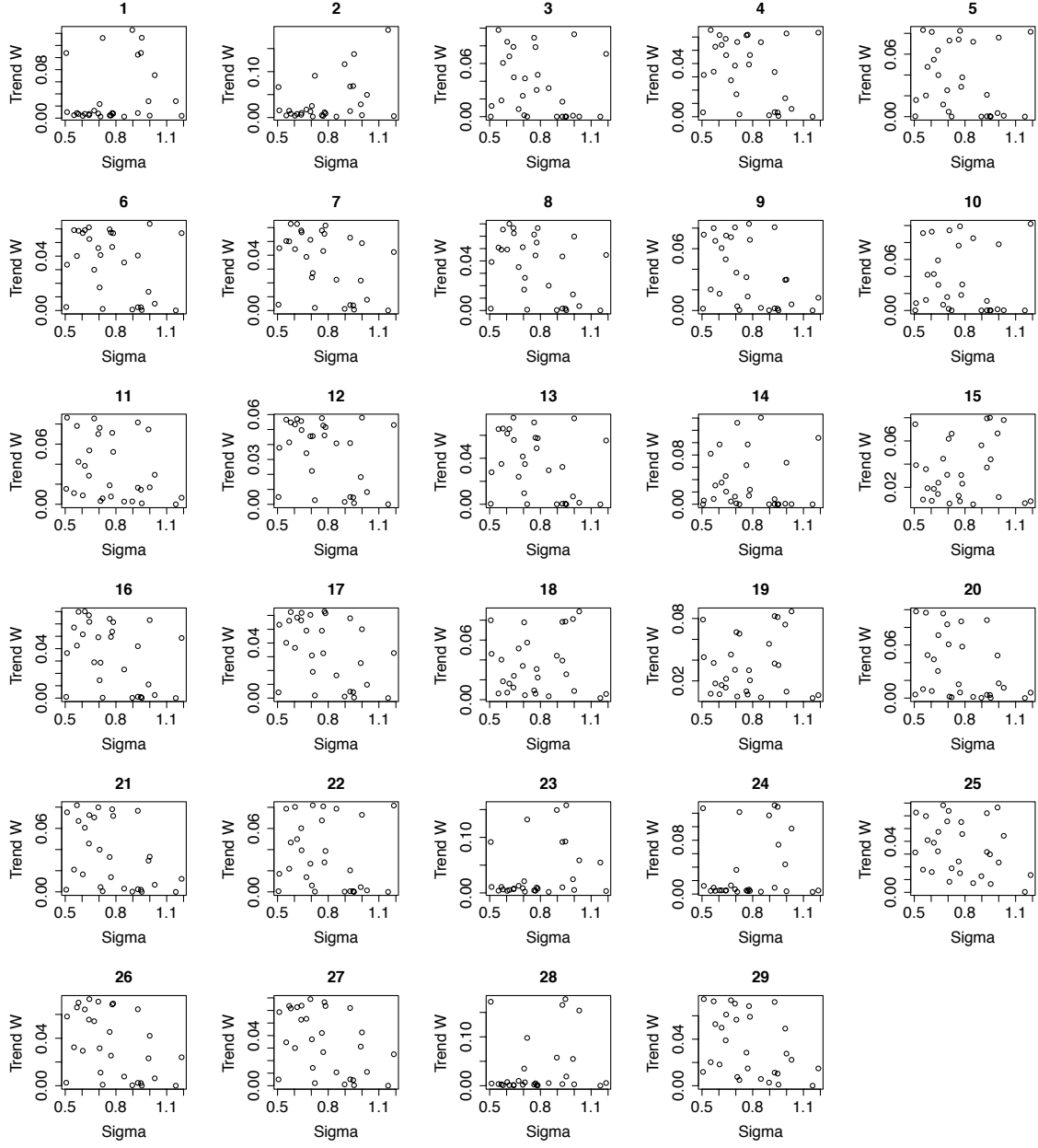


Figure S6. Same as Figure S2, but for un-normalized standard deviation [K] and the Korea_temp_long experiment.

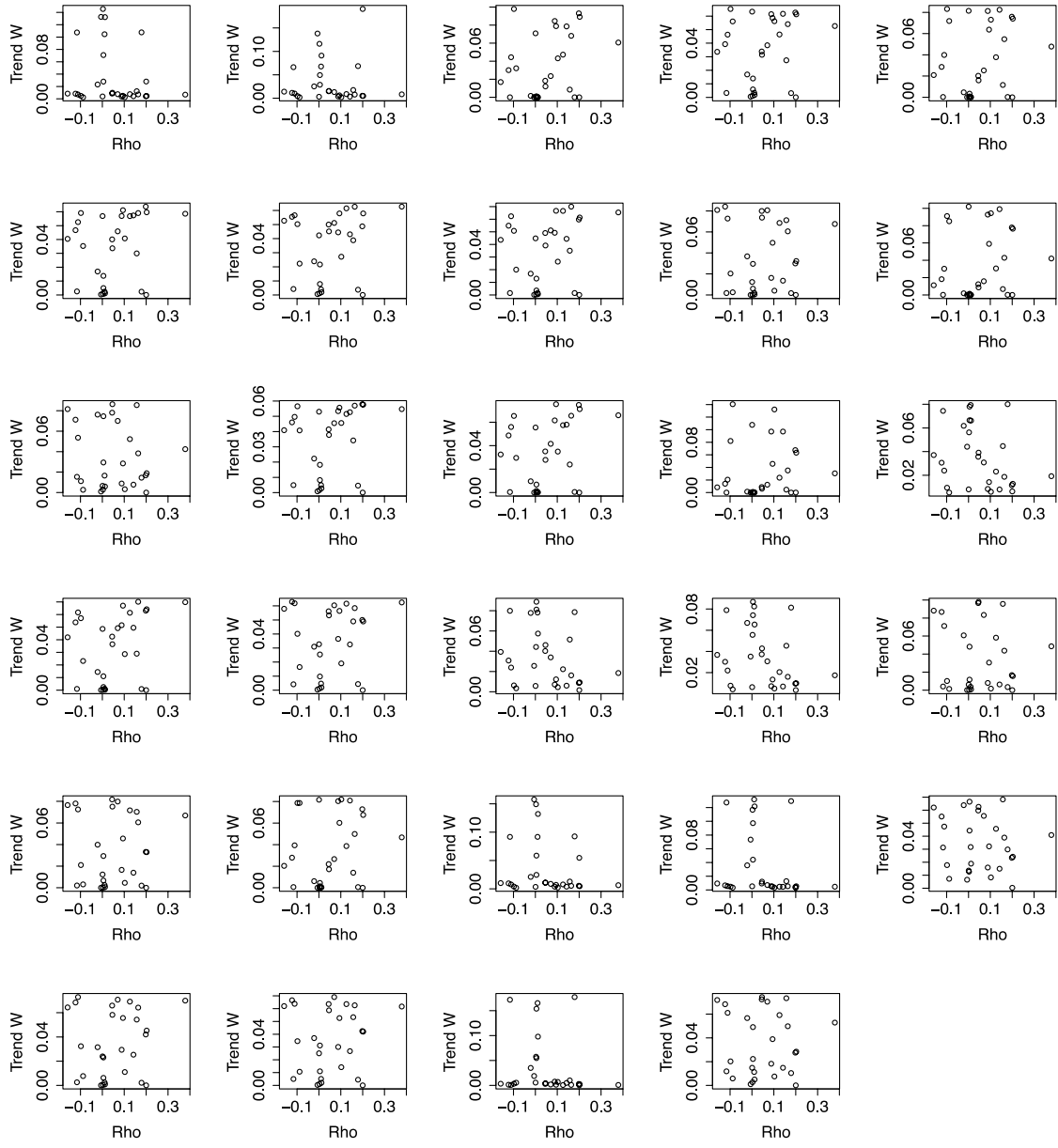


Figure S7. Same as Figure S3, but for the Korea_temp_long experiment.

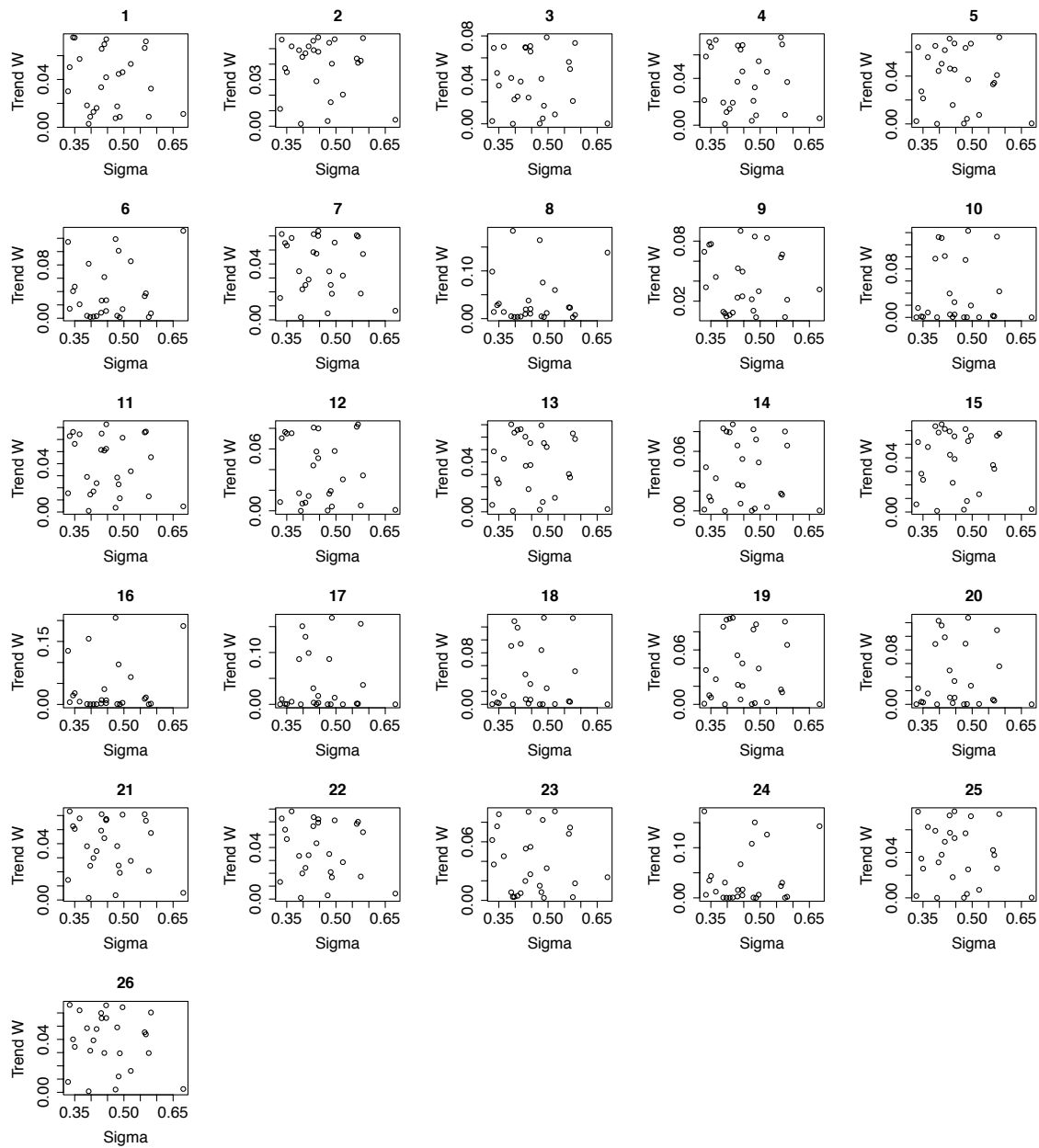


Figure S8. Same as Figure S2, but for un-normalized standard deviation [K] and the Winter_SST experiment.

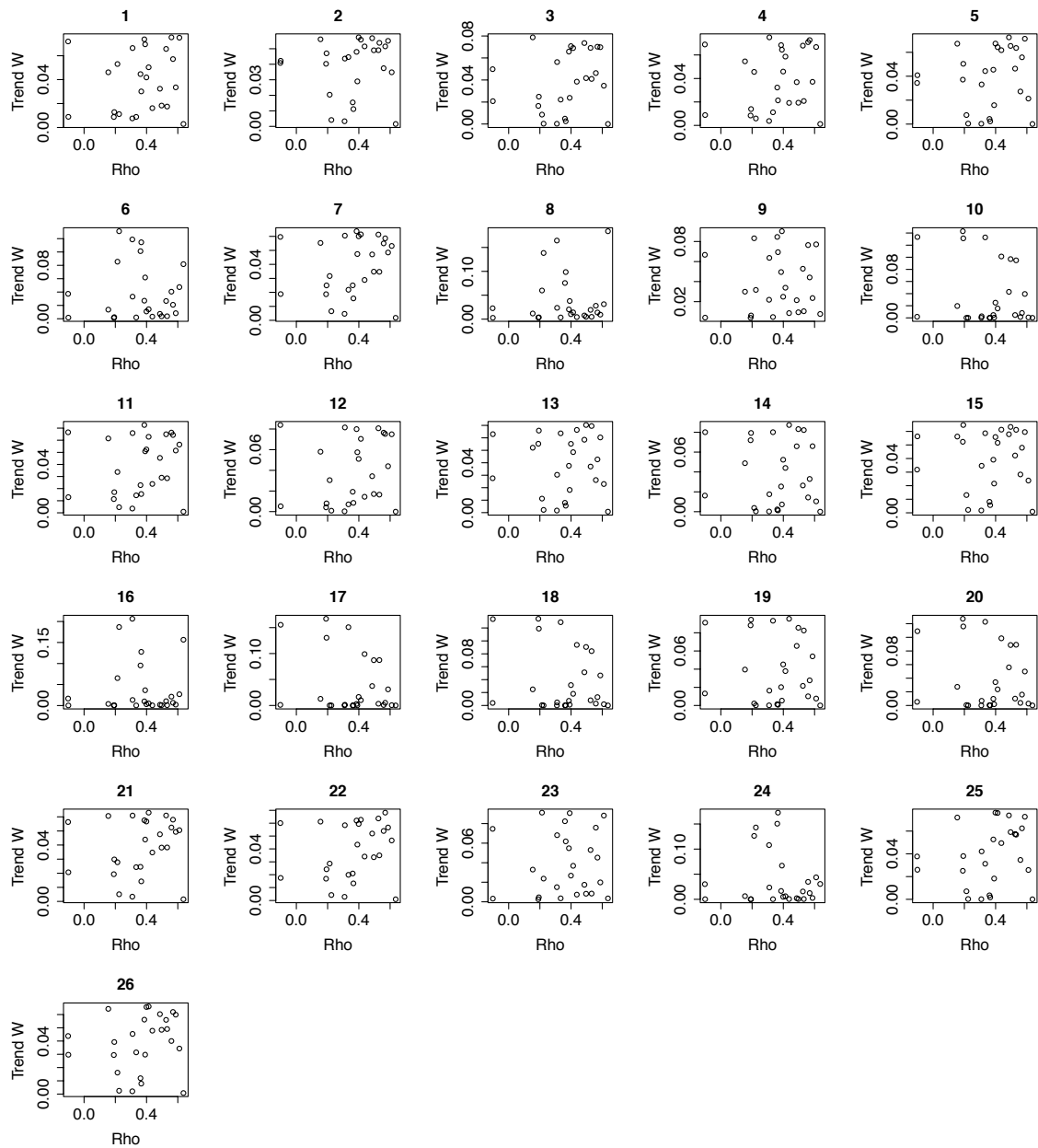


Figure S9. Same as Figure S3, but for the Winter_SST experiment.

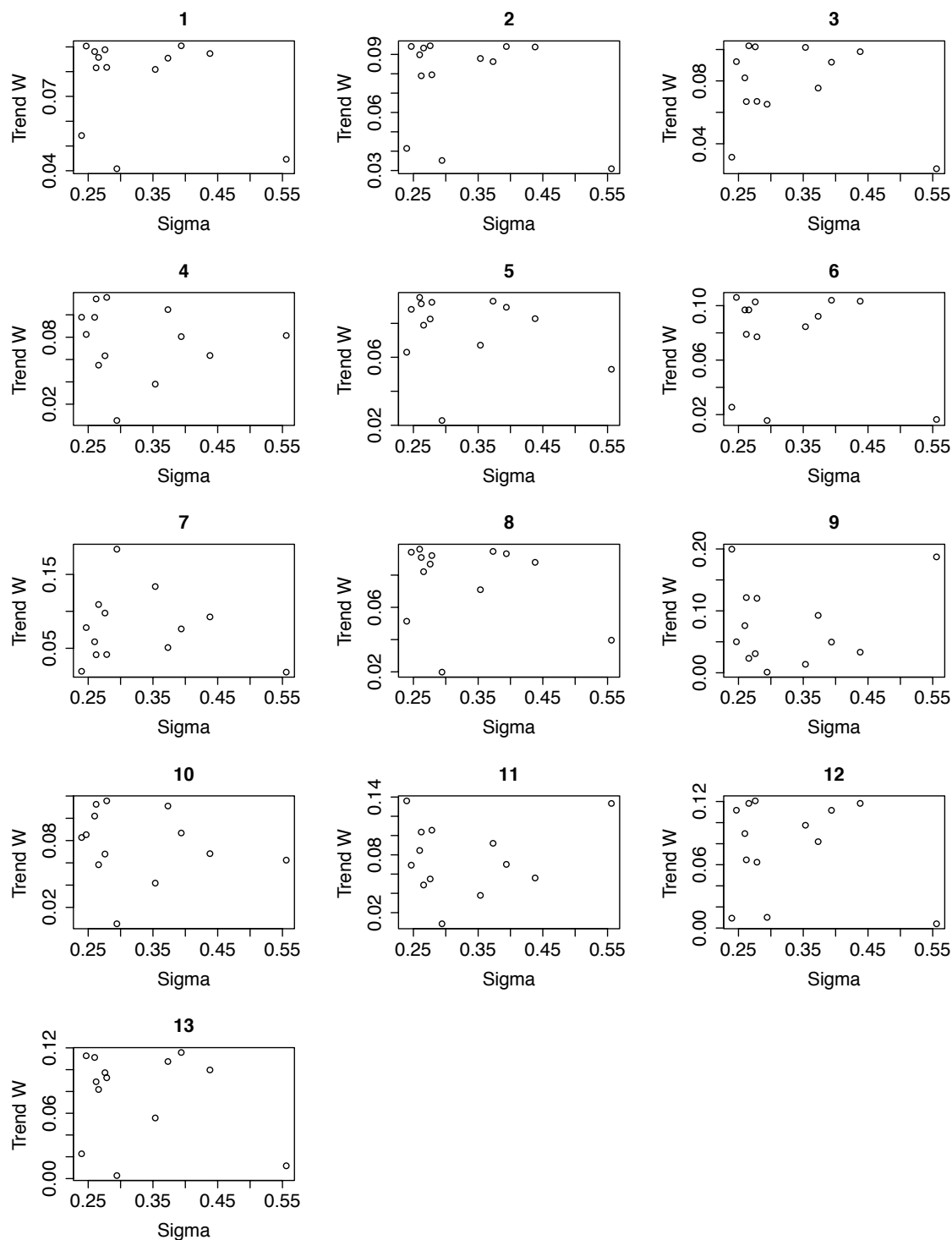


Figure S10. Same as Figure S2, but for un-normalized standard deviation [K] and the AMOCIndex experiment.

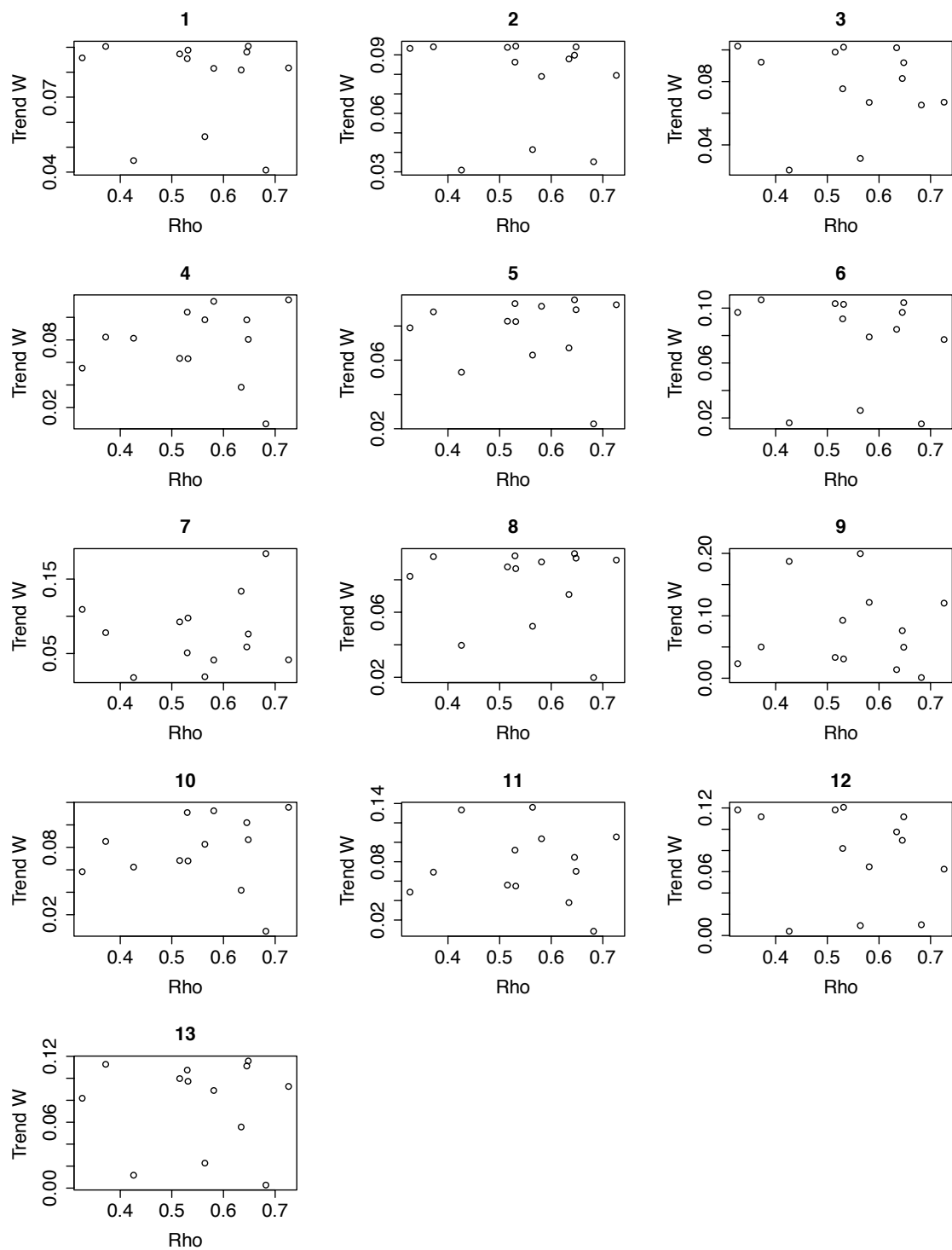


Figure S11. Same as Figure S3, but for the AMOCIndex experiment.

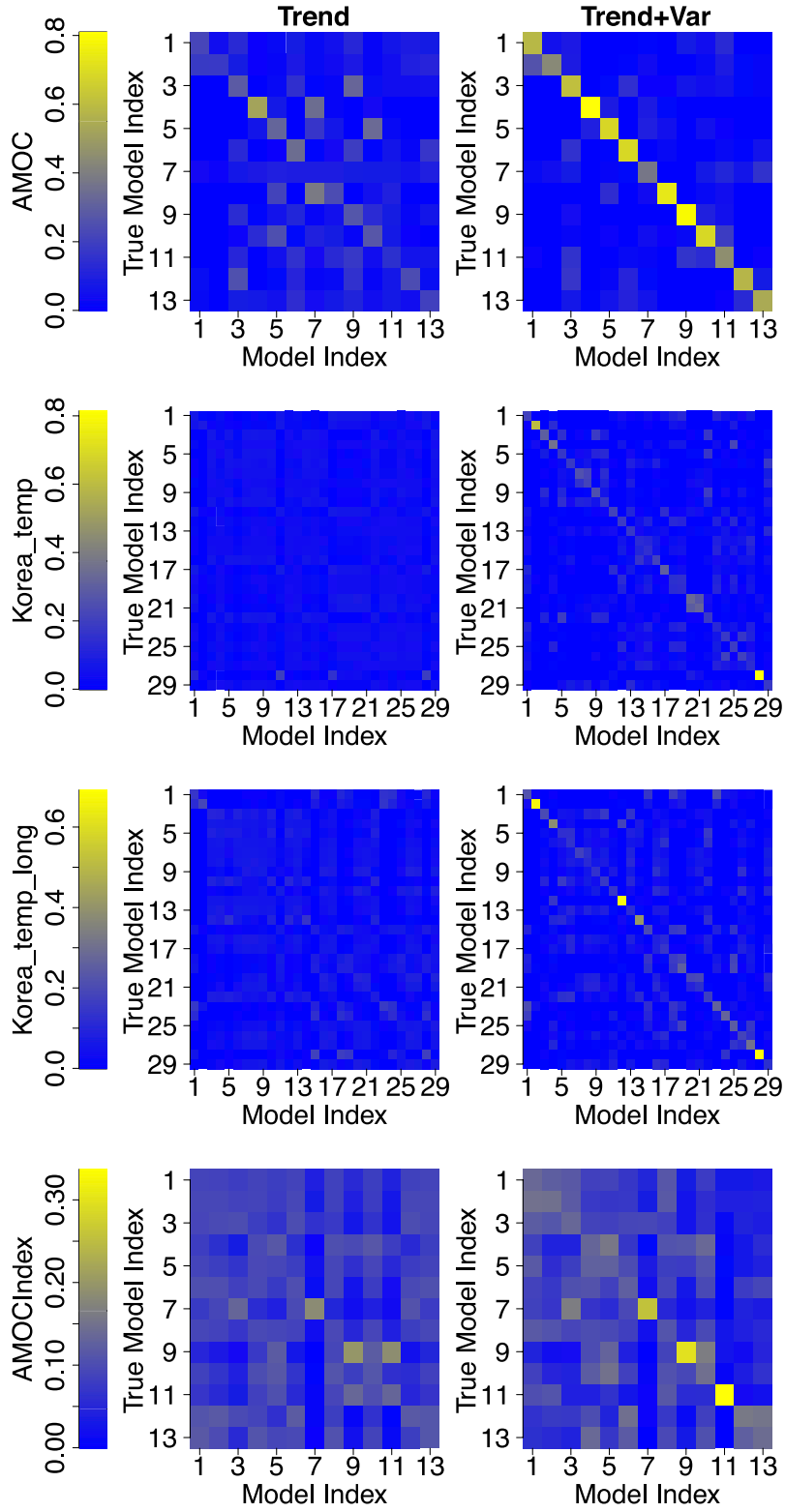


Figure S12. Similar to Figure 5, but for the rest of one-at-a-time cross-validation experiments.

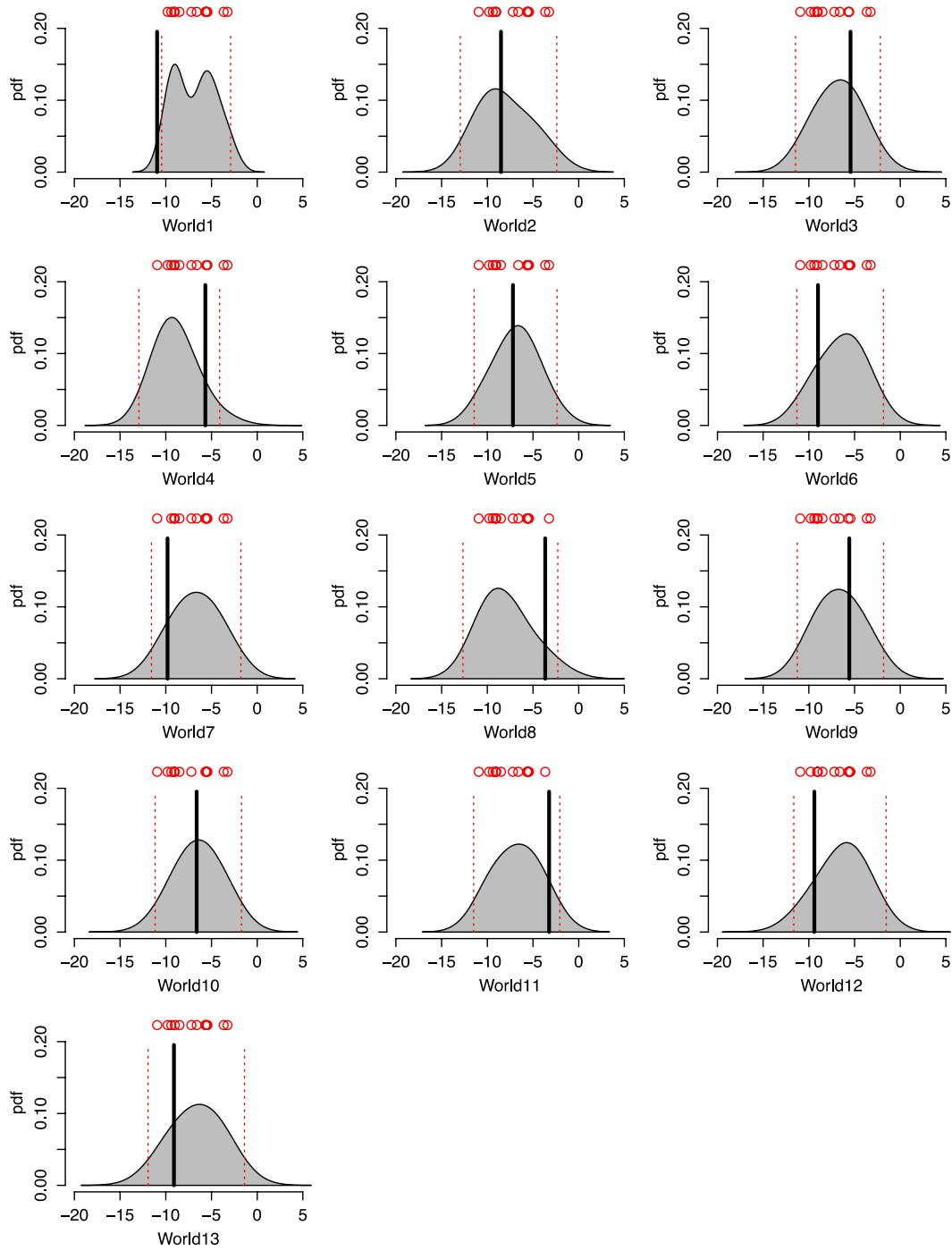


Figure S13. Probabilistic projections for AMOC change from 1960-1999 to 2060-2099 [Sv] under the RCP8.5 emissions scenario for the “trend” AMOC cross-validation experiment. Subplots differ in the assumed “true” model. Red circles are deterministic projections from each model, red dotted lines are 90% posterior credible intervals. Black lines are changes from the “true” models.

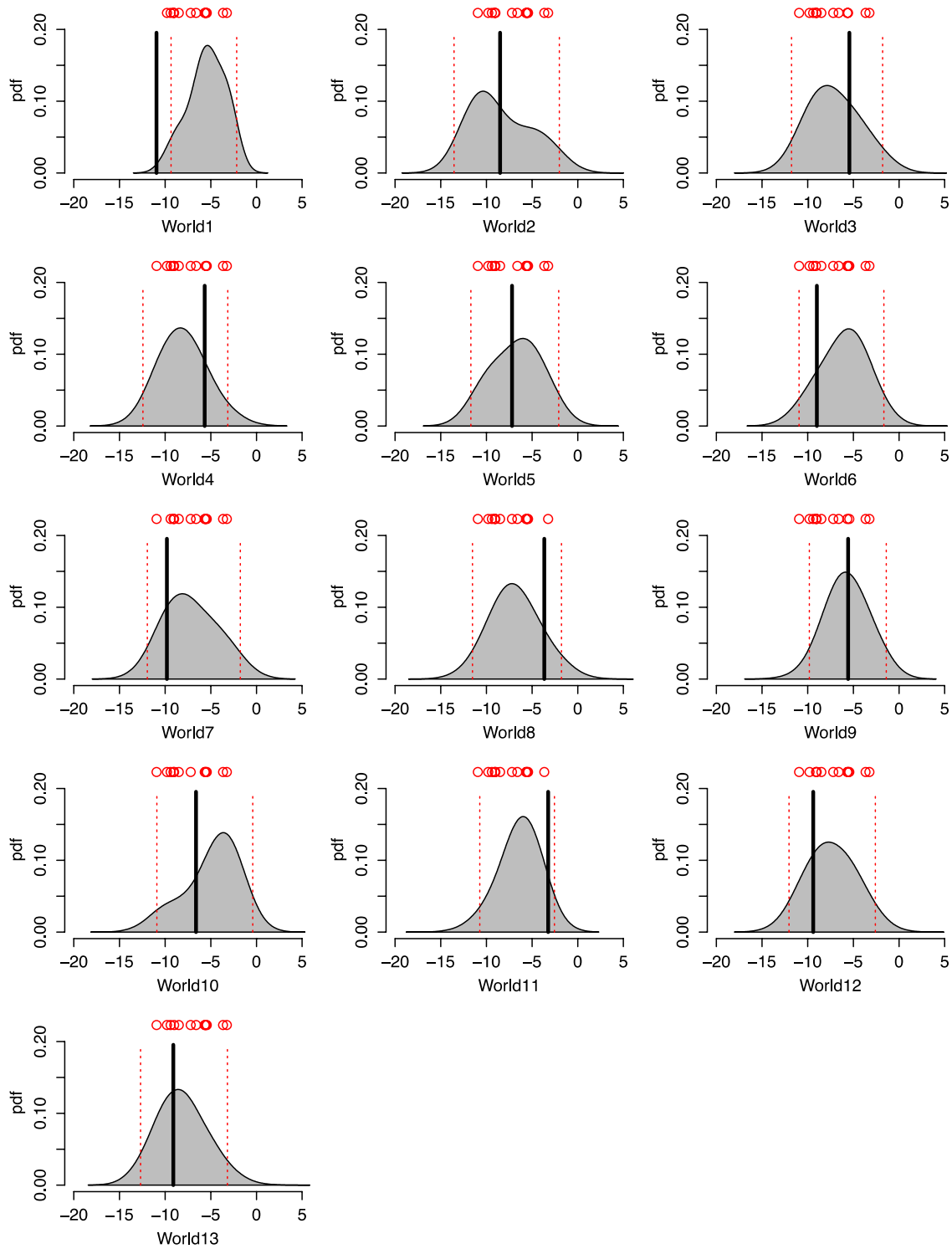


Figure S14. Similar to Figure S13, but for the AMOC “trend+var” experiment.

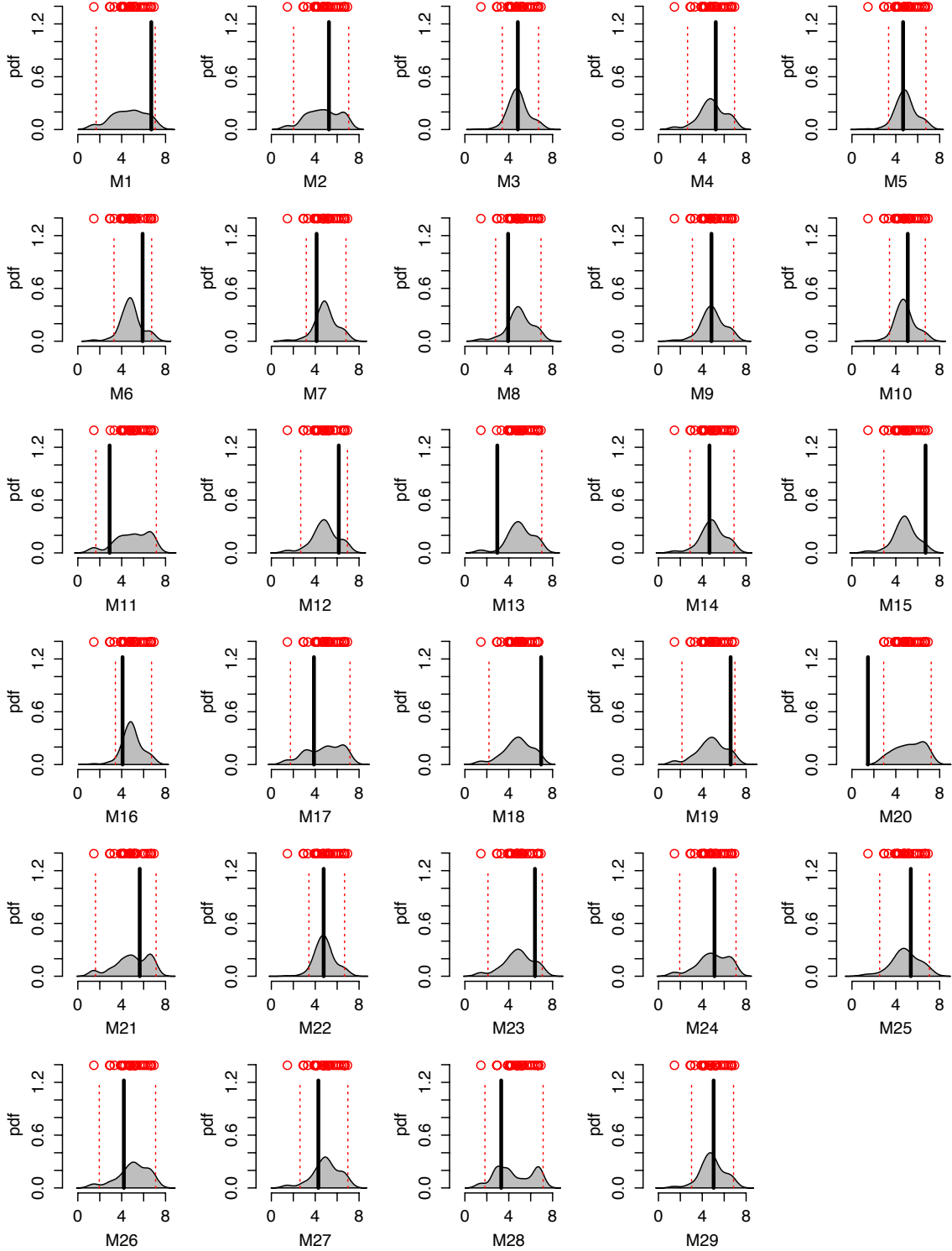


Figure S15. Similar to Figure S13, but for the Korea_temp “trend” experiment. The pdfs represent Korean JJA mean maximum temperature change from 1973-2005 to 2081-2100 [K] under the RCP8.5 emissions scenario.

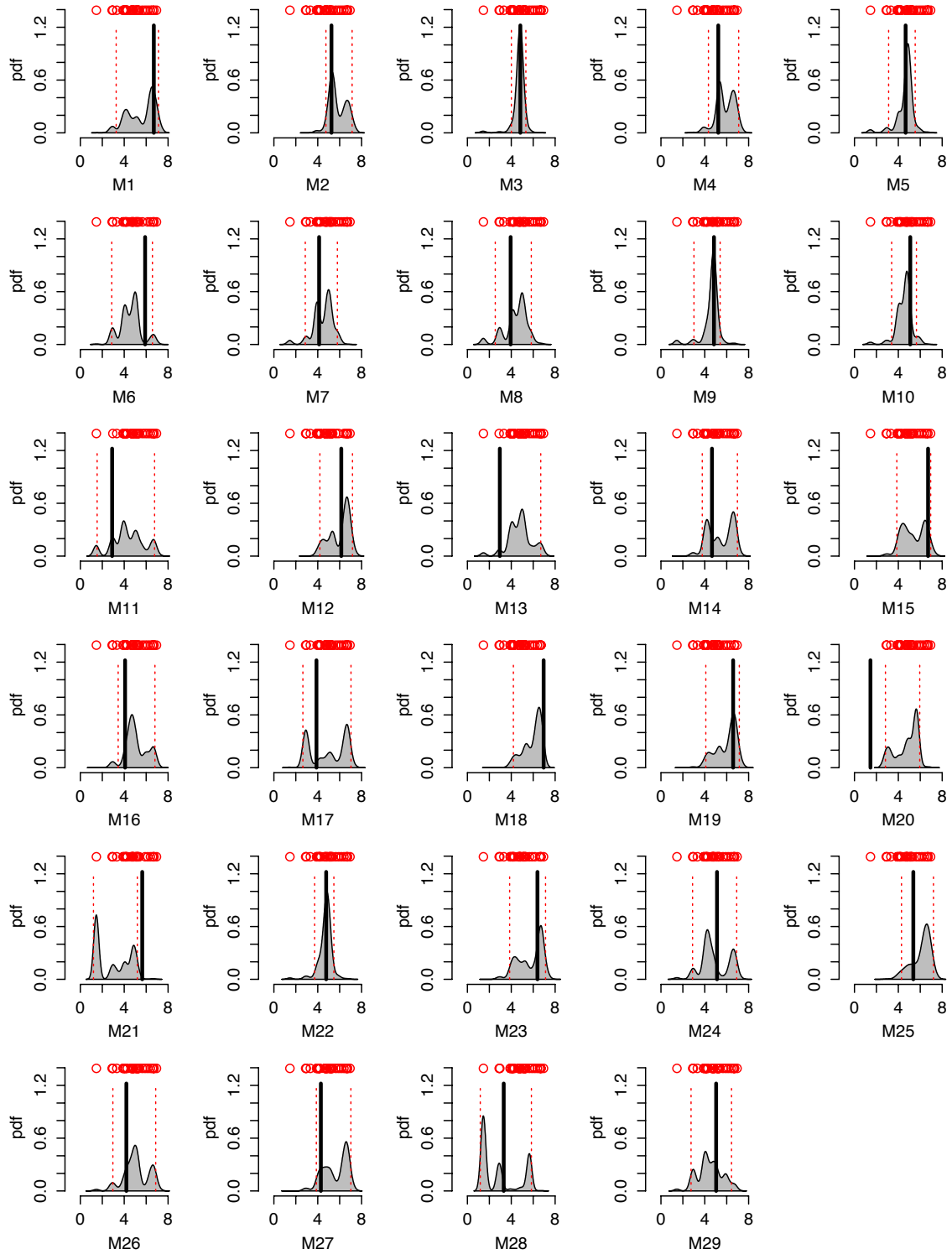


Figure S16. Similar to Figure S15, but for the Korea_temp “trend+var” experiment.

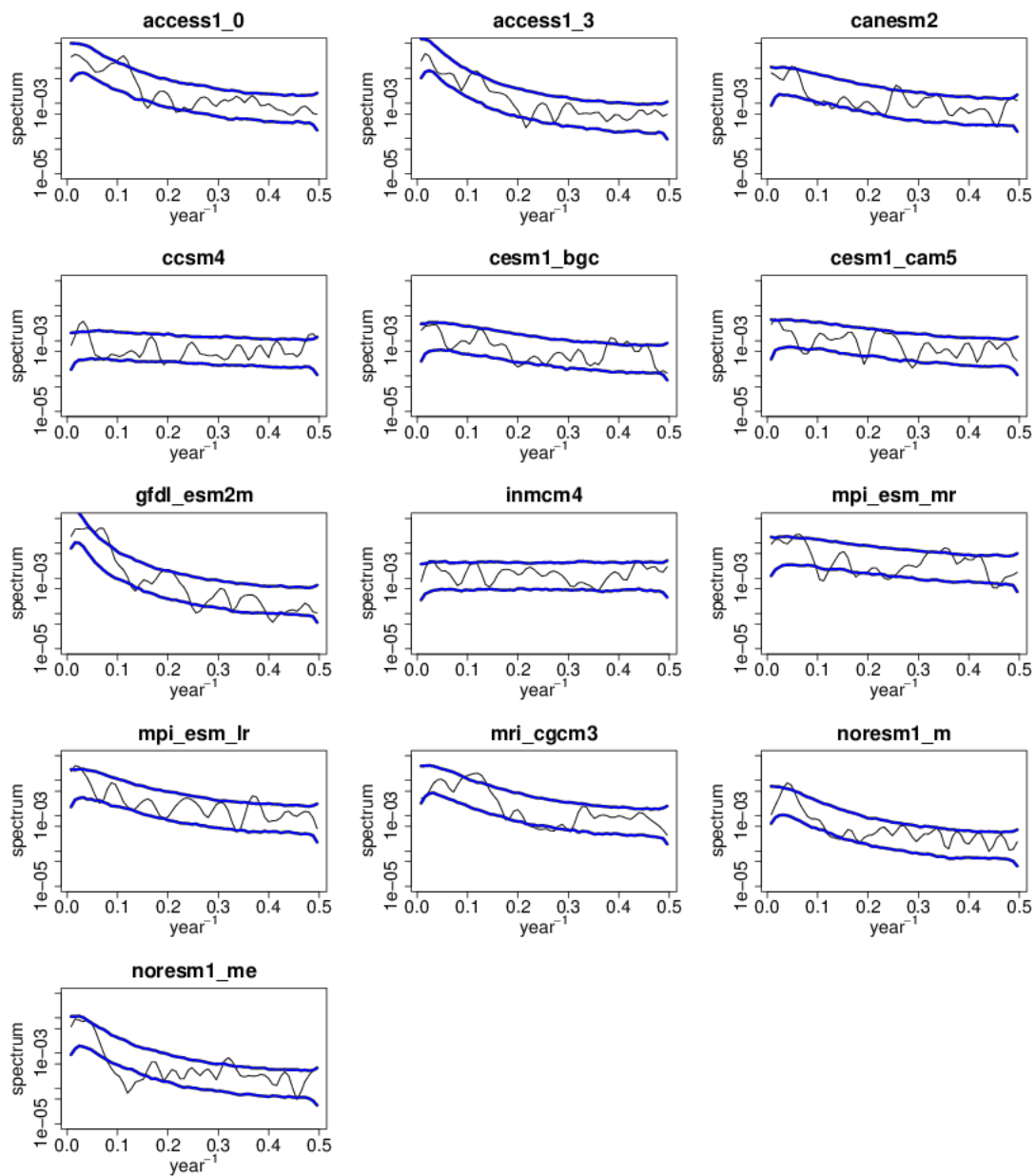


Figure S17. Spectra plots for AMOC experiment model fluctuations for years 1880-2004. Blue lines: 90% confidence intervals for spectra of an AR1 process that was fit to modelled fluctuations, using 1000 realizations. *Y*-axis is logarithmic.

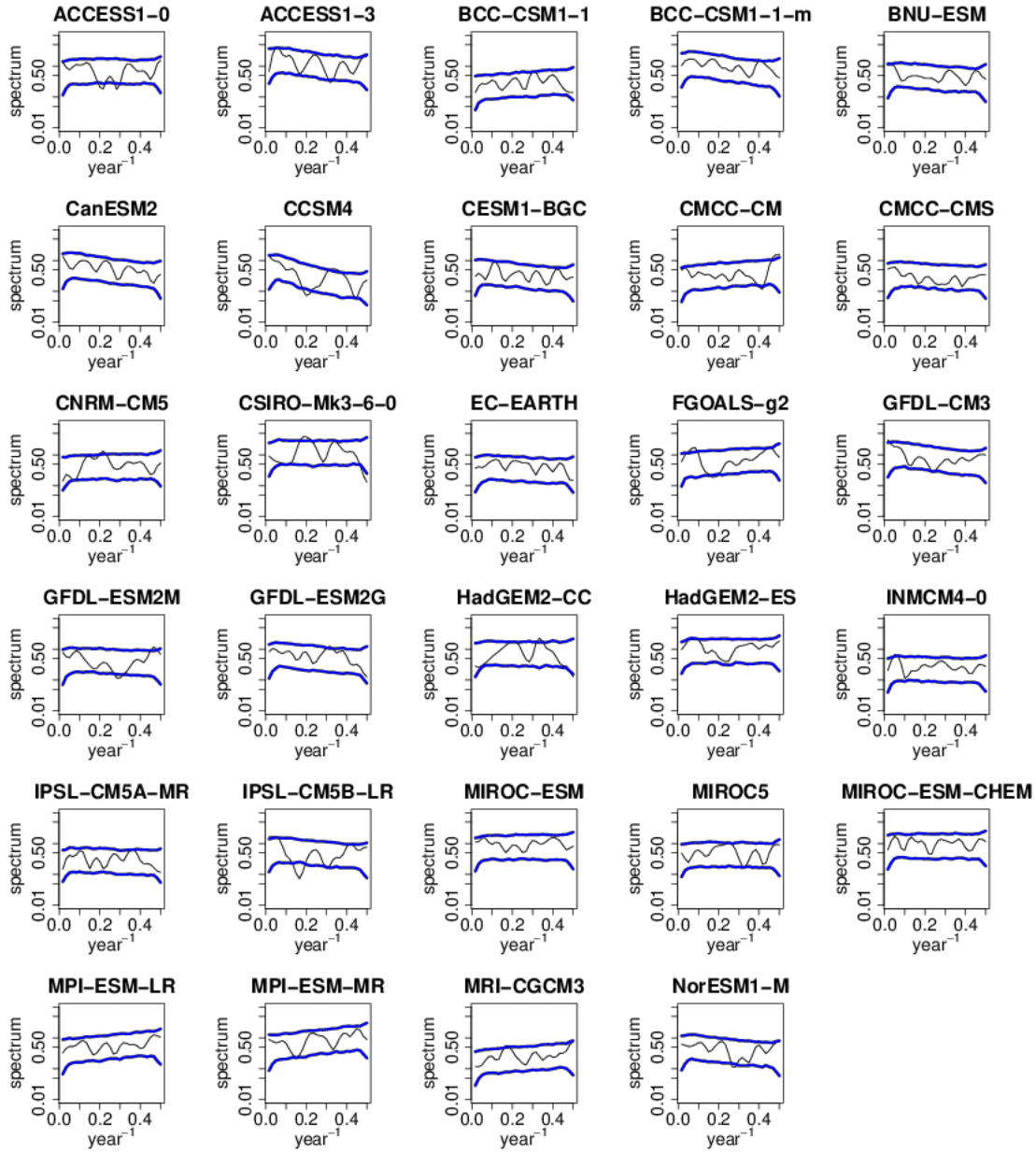


Figure S18. Same as Figure S17 but for Korea_temp_long experiment model fluctuations for years 1950-2005. Y-axis is logarithmic.

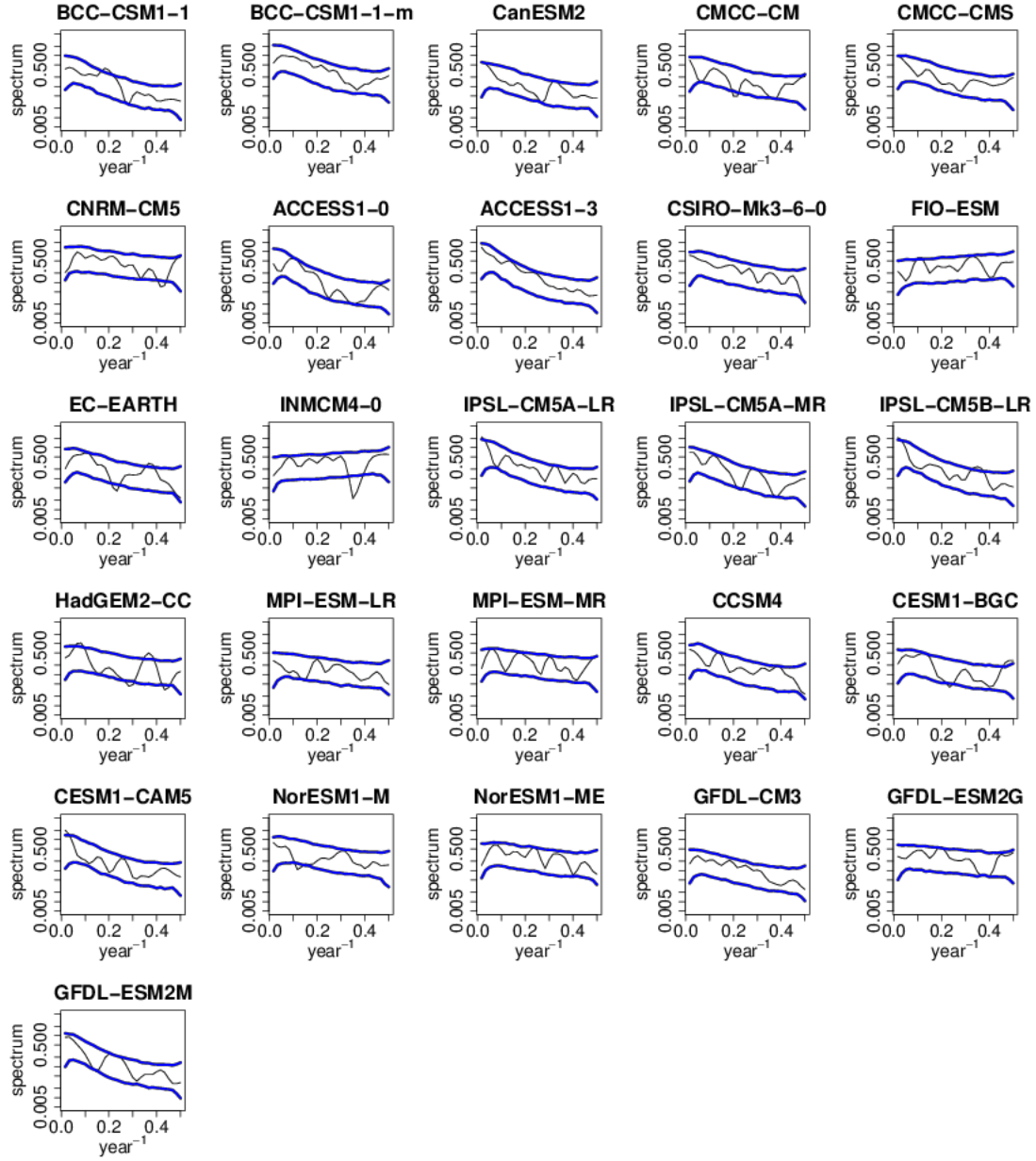


Figure S19. Same as Figure S17 but for Winter_SST_ experiment model fluctuations for years 1941-2000. Y-axis is logarithmic.

Model Number	Name	Modeling Centre
1	ACCESS1-0	CSIRO and BOM, Australia
2	ACCESS1-3	CSIRO and BOM, Australia
3	bcc-csm1-1	Beijing Climate Center & China Meteorological Administration, China
4	bcc-csm1.1-m	Beijing Climate Center & China Meteorological Administration, China
5	BNU-ESM	Beijing Normal University, China
6	CanESM2	Canadian Centre for Climate Modeling and Analysis, Canada
7	CCSM4	National Center for Atmospheric Research, USA
8	CESM1-BGC	National Science Foundation, Department of Energy, National Center for Atmospheric Research, USA
9	CMCC-CM	Euro-Mediterranean Centre on Climate Change, Italy
10	CMCC-CMS	Euro-Mediterranean Centre on Climate Change, Italy
11	CNRM-CM5	National Centre for Meteorological Research & European Centre for Research and Advanced Training in Scientific Computation, France
12	CSIRO-Mk3-6-0	Queensland Centre for Climate Change Excellence & CSIRO, Australia
13	EC-EARTH	EC-Earth consortium, Europe
14	FGOALS-g2	Institute of Atmospheric Physics, Chinese Academy of Sciences, China
15	GFDL-CM3	Geophysical Fluid Dynamics Laboratory, USA
16	GFDL-ESM2M	Geophysical Fluid Dynamics Laboratory, USA
17	GFDL-ESM2G	Geophysical Fluid Dynamics Laboratory, USA
18	HadGEM2-CC	Met Office Hadley Centre, UK
19	HadGEM2-ES	Met Office Hadley Centre, UK
20	inmcm4-0	Institute of Numerical Mathematics, Russia
21	IPSL-CM5A-MR	Institute Pierre Simon Laplace, France
22	IPSL-CM5B-LR	Institute Pierre Simon Laplace, France
23	MIROC-ESM	University of Tokyo, National Institute for Environmental Studies & Japan Agency for Marine-Earth Science and Technology, Japan
24	MIROC5	University of Tokyo, National Institute for Environmental Studies & Japan Agency for Marine-Earth Science and Technology, Japan
25	MIROC-ESM-CHEM	University of Tokyo, National Institute for Environmental Studies & Japan Agency for Marine-Earth Science and Technology, Japan
26	MPI-ESM-LR	Max Planck Institute for Meteorology (MPI-M), Germany
27	MPI-ESM-MR	Max Planck Institute for Meteorology (MPI-M), Germany
28	MRI-CGCM3	Meteorological Research Institute, Japan

29	NorESM1-M	Norwegian Climate Centre, Norway
----	-----------	----------------------------------

Table S1: Basic information about GCMs used for the Korea_temp and Korea_temp_long experiments.

Model Number	Name	Modeling Centre
1	bcc-csm1-1	Beijing Climate Center & China Meteorological Administration, China
2	bcc-csm1.1-m	Beijing Climate Center & China Meteorological Administration, China
3	CanESM2	Canadian Centre for Climate Modeling and Analysis, Canada
4	CMCC-CM	Euro-Mediterranean Centre on Climate Change, Italy
5	CMCC-CMS	Euro-Mediterranean Centre on Climate Change, Italy
6	CNRM-CM5	National Centre for Meteorological Research & European Centre for Research and Advanced Training in Scientific Computation, France
7	ACCESS1-0	CSIRO and BOM, Australia
8	ACCESS1-3	CSIRO and BOM, Australia
9	CSIRO-Mk3-6-0	Queensland Centre for Climate Change Excellence & CSIRO, Australia
10	FIO-ESM	The First Institute of Oceanography, SOA, China
11	EC-EARTH	EC-Earth consortium, Europe
12	inmcm4-0	Institute of Numerical Mathematics, Russia
13	IPSL-CM5A-LR	Institute Pierre Simon Laplace, France
14	IPSL-CM5A-MR	Institute Pierre Simon Laplace, France
15	IPSL-CM5B-LR	Institute Pierre Simon Laplace, France
16	HadGEM2-CC	Met Office Hadley Centre, UK
17	MPI-ESM-LR	Max Planck Institute for Meteorology (MPI-M), Germany
18	MPI-ESM-MR	Max Planck Institute for Meteorology (MPI-M), Germany
19	CCSM4	National Center for Atmospheric Research, USA
20	CESM1-BGC	National Science Foundation, Department of Energy, National Center for Atmospheric Research, USA
21	CESM1-CAM5	National Science Foundation, Department of Energy, National Center for Atmospheric Research, USA
22	NorESM1-M	Norwegian Climate Centre, Norway
23	NorESM1-ME	Norwegian Climate Centre, Norway
24	GFDL-CM3	Geophysical Fluid Dynamics Laboratory, USA
25	GFDL-ESM2G	Geophysical Fluid Dynamics Laboratory, USA
26	GFDL-ESM2M	Geophysical Fluid Dynamics Laboratory, USA

Table S2. Basic information about GCMs used for the Winter_SST experiment.